To the Graduate Council:

I am submitting herewith a thesis written by Cheng Luo entitled "Fiber Surface Characterization by Laser Back Scattering." I have examined the final copy of this thesis for form and content and recommend that it be accepted in partial fulfillment of the requirements for the degree of Master of Science, with a major in Textiles and clothing.

Randall R. Bresee, Major Professor

We have read this thesis and recommend its acceptance:

K. E. Duckett

Larry C. Wadsworth

M. J. Robo

Accepted for the Council:

Vice Provost
and Dean of the Graduate School

FIBER SURFACE CHARACTERIZATION BY LASER BACK SCATTERING

A Thesis
Presented for the
Master of Science
Degree
The University of Tennessee, Knoxville

Cheng Luo

May, 1989

ACKNOWLEDGEMENTS

The author wishes to express his thanks and appreciation to Dr. Randall R. Bresee for his guidance and efforts throughout this study. Appreciation is also extended for their guidance to Dr. Michael J. Roberts, Dr. Kermit E. Duckett, and Dr. Larry C. Wadsworth, who served as committee members.

Special thanks are given to Dr. John F. Fellers and Mr. Larry J. Effler for their guidance and providing the necessary facilities within the SALS laboratory of the Material Science and Engineering Department and to my fellow graduate students for moral support.

Deepest appreciation is extended to the author's parents, Mr. and Mrs. H. D. Cheng for their support and encouragement.

ABSTRACT

Fiber surface structure is important because it affects the behavior of fibers, yarns and fabrics during their processing as well as during their use in service. For example, the geometric roughness of a fiber's surface greatly affects frictional characteristics and luster of the fiber or yarns and fabrics made from the fiber.

Since the advent of lasers, scattering phenomena have received considerable attention both theoretically and experimentally. According to the theory of Fourier optics, the far-field diffraction pattern is the Fourier transform of the diffracting object. This can be postulated to back scattering also. Therefore, one ought to be able to obtain information about the surface structure of materials from their laser back scattering patterns. The application of laser back scattering to fiber surface roughness characterization was studied in this thesis from both theoretical and experimental approaches. This study reveals relationships between back scattering patterns and fiber surface roughness.

In order to quantify experimentally measured roughness, a parameter called the "roughness coefficient" was defined as the ratio of scattered intensities at non-zero spatial frequencies to the intensity at zero spatial frequency. A computer simulation study was employed to investigate the theoretical influence of root-mean-square fiber surface roughness, fiber cross-sectional shapes, fiber diameters and surface asperity shapes on back scattering patterns.

Two instruments were employed to measure fiber surface roughness based on optical Fourier transforms. The first one used a vidicon-camera to capture the scattering pattern and provide input to a micro-computer for data analysis. The second simpler instrument consisting of a few of photo-detectors were used to reduce cost. Several applications of laser back scattering have been examined, such as measuring the effect of "delustering" fibers with T_iO_2 and detecting surface crystallization. The optical transform method discussed in this study seems to have potential as a simple means of providing nonintrusive, real- time measurements of fiber surface structure during processing or after use in service.

TABLE OF CONTENTS

LIST OF FIGURES

LIST OF TABLES

CHAPTER I

INTRODUCTION

Fiber surface structures are important because of their effects on textile behavior during processing and performance of finished products. Prominent among surface characteristics is geometric roughness since it is closely related to frictional and optical properties. Frictional properties influence mechanical properties of textiles and fabric hand, whereas optical properties affect the appearance of fabrics.

A thorough investigation of fiber geometric roughness must include determining the distribution of variously sized asperities on the surface. The size of these asperities may vary from macroscopic to molecular magnitudes. However, they all contribute in some degree to the overall properties of the fiber. In the past forty years, work has been done in this field but results were limited by the experimental techniques.

Since the advent of lasers, scattering phenomena produced by coherent laser light have received considerable attention and many investigators have studied theoretical and experimental aspects of scattering. This thesis will provide an introduction to laser scattering and discuss its applications to the characterization of fiber surface geometric roughness.

OBJECTIVES

The objectives of this study were:

1. To develop a method to characterize fiber surface roughness which is simple, accurate, inexpensive to perform, and is based on optical Fourier transform theory.

2. To investigate relationships between fiber surface structure and scattering patterns.

3. To use optical transforms to explore applications of fiber geometric roughness measurements including

A. effects of fiber delustering with T_iO_2 on surface roughness.

B. use of surface roughness measurements to determine crystallization rates.

CHAPTER II

REVIEW OF LITERATURE AND THEORY

2.1 SMOOTH AND ROUGH SURFACES

The surface profile of a rough surface along one dimension can be represented as shown in Figure 2.1 by its coordinates with respect to an ideal smooth reference plane. For simplicity, surface profiles can be expressed in a statistical manner by the root-mean-square roughness, defined as

$$\sigma_{rms} = [\frac{1}{N}\sum_{i=1}^{N}(y_i - \overline{y})^2]^{1/2} \qquad (2.1)$$

where σ is the RMS roughness, N is the number of height data points,y_i is the height of point i with respect to the reference plane denoted by the horizontal straight line, and $\overline{y}$ is the mean of all height data points[1].

What is smooth and what is rough? Perhaps the most striking difference between smooth and rough surfaces is the fact that a smooth surface will reflect incident light specularly in a single direction whereas a rough surface will scatter it into numerous directions[2].

Rough surfaces can be divided into two classes: surface with exactly given regularly repeating profiles such as sinusoidal undulations, saw-tooth profiles or regular corrugations, and surfaces with random irregularities. There are also many surfaces which are mixtures of these two.

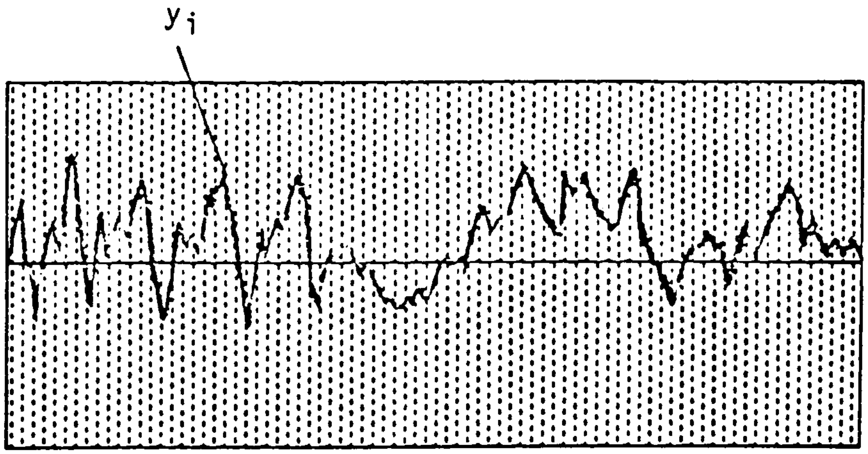

Figure 2.1: One-dimensional surface profile [1].

According to this view of roughness, specular reflection and diffuse scattering provide a convenient measure of roughness. Considering Figure 2.2, all of the light incident on the surface "A" is specularly reflected, as from a smooth mirror. In this case, the angle of incidence, i, equals the angle of reflection, r, and both the original and the reflected rays lie in the plane perpendicular to the surface. The great majority of surfaces, however, lack the polished uniformity of a smooth mirror and minute irregularities scatter the incident light in all directions. The extreme case is diffuse reflection is shown for surface "B", and the surface would appear to be equally well illuminated when viewed from any angle. A third type

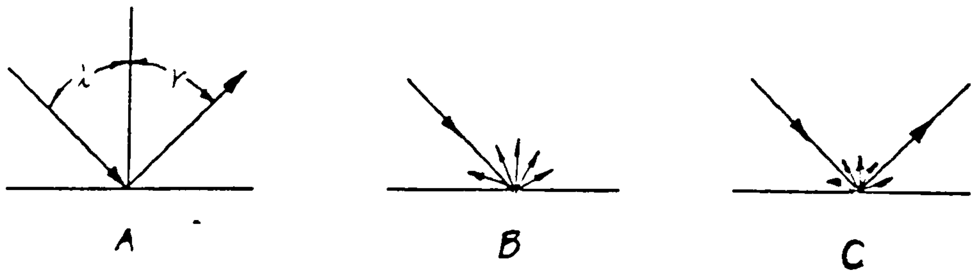

Figure 2.2: Three types of surface [3].

of reflection is illustrated in "C" and is a combination of A and B. Although some of the incident light is reflected diffusely, the intensity of reflected light is greatest at the angle of specular reflection[3].

Luster is a general term used to describe light reflection from textiles. It is a phenomenon involving contrasts between bright (highly reflective) areas and a darker (diffuse) background, as represented by case C. However, many other factors contribute to the perception of luster in textiles, including physiological and psychological factors. The basic optical quantity determining luster is directional reflectance. Hunter[4,5] and Fourt[7] have evaluated luster using a ratio of specular reflectance and diffuse reflectance components. When the reflectance of the diffuse and specular components are the same, the ratio is 1.0 and the surface is said to exhibit zero gloss. Comparing this with the definition of roughness given by Beckmanm[2], luster and roughness have a common nature.

2.2 FIBER SURFACE ROUGHNESS IN RELATION TO LINEAR ASSEMBLIES DURING PROCESSING

During staple yarn manufacturing, each fiber interacts with its neighbors to affect the general fiber alignment. The behavior and migration of staple fiber during processing is reflected in yarn properties. Depending on processing conditions, the cohesion of staple fiber assemblies can either enhance or prevent uniform drafting. The cohesion of loose structures, such as sliver and roving depends highly on fiber surface contacts and characteristics.

Scardino and Lyons[8] have studied the influence of fiber surface roughness on the mechanical properties of assemblies during processing. As indicated by performance during opening processes, geometrically smooth fibers were found to be more difficult to separate from one another. The rougher fibers appeared to open much easily and more thoroughly than the smooth fibers in the same number of operations. In subsequent processes, smooth fibers lead to greater cohesion in fiber assemblies. This was found to lead to reduced actual drafts under certain processing conditions. Similarly, in blends of smooth and rough fibers in slivers, the cohesion was found to increase consistently with increasing percentage of smooth fibers.

2.3 LUSTER

Luster was the subject of a great deal of investigation during the 1950's and 1960's. In 1949, Buck[3], discussed the market demand for luster in cotton and summarized the technical background of the subject. Beginning in 1951, Fourt[7] at al. published a series of reports on improving luster in cotton. Since the judging of luster is a subjective combination of visual impressions, the central problem of luster measurement is to obtain physical measurements which correspond to these visual impressions and can be combined to correlate with the overall judgment. Several analytical methods have been developed for this.

Nickerson[9] developed a single-answer, direct-reading instrument especially adapted for measuring luster of raw cotton fiber and yarns. The sample is illuminated at 45^o and reflected light is measured at 0^o (nonspecular) and 45^o (specular). By means of a special circuit, the ratio of these two measurements may be read directly in terms of "percent luster".

Holboke and Berriman[10] studied light scattering from fibers. An instrument was constructed to measure the angle and intensity of light scattered from single fibers. The principle was based on the depolarization effect, which can be explained in this way: The light scattered from an object may be thought of as consisting of coherent and incoherent components. The coherent portion retains the particular characteristics of the source, such as its polarization state, whereas the incoherent portion appears to originate directly from the object and has no relation to the original source. By means of aligning or crossing polarizers, the coherency can be determined from:

$$\alpha = (I_a - I_c)/(I_a + I_c) \qquad (2.2)$$

where α=coherency, I_a=intensity measured with polarizers aligned parallel, and I_c=Intensity measured with polarizers crossed.

Results showed that coherency decreased as luster decreased. Since depolarization apparently is an indicator of luster, the fiber qualities that cause depolarization should also control luster. Experiments showed that a small degree of surface roughness is very effective in decreasing the luster.

A similar principle was used by Jeffries[6] in an instrument designed to measure "deluster" in woven filament fabrics. He also discussed the reflection of unpolarized light and of plane-polarized light in relation to the effect of delustering.

2.4 METHODS TO EVALUATE ROUGHNESS

Over the past 30 years, a number of research groups have studied surface roughness of metals. The measurement techniques may be considered to be either contact or noncontact. The most common contact technique employs a stylus profilometer. Noncontact methods are optical methods, the two major ones being speckle contrast and optical transform techniques.

2.4.1 CONTACT METHOD: STYLUS PROFILOMETER

The stylus profilometer has a long history in metallic surface measurement. About twenty years ago, it was adapted to measure fiber surface roughness[11]. At first, a technique was used that depended upon electrical amplification of the motion of a stylus perpendicular to the surface being drawn across the stylus as shown in Figure 2.3. Later, a transducer providing increased sensitivity based on the principle of generating a voltage by the rotation of a coil in a magnetic field was used.

The disadvantage of stylus methods are that the stylus may damage the test surface, sensitivity is comparatively low and the resolution is limited by the finite radius of curvature of the stylus. In addition, the stylus profilometer gives only one-dimensional information about the surface roughness of the object.

2.4.2 NONCONTACT METHOD : SPECKLE CONTRAST

During the mid 1970's, the speckle produced by coherent laser light has been investigated by many researchers. Statistical properties of speckle patterns in the diffraction and image fields of a diffusely transmitting or reflecting object have received special attention[12-20]. Asakura et al[14] have performed extensive theoretical and experimental studies of the statistical properties of speckle intensity

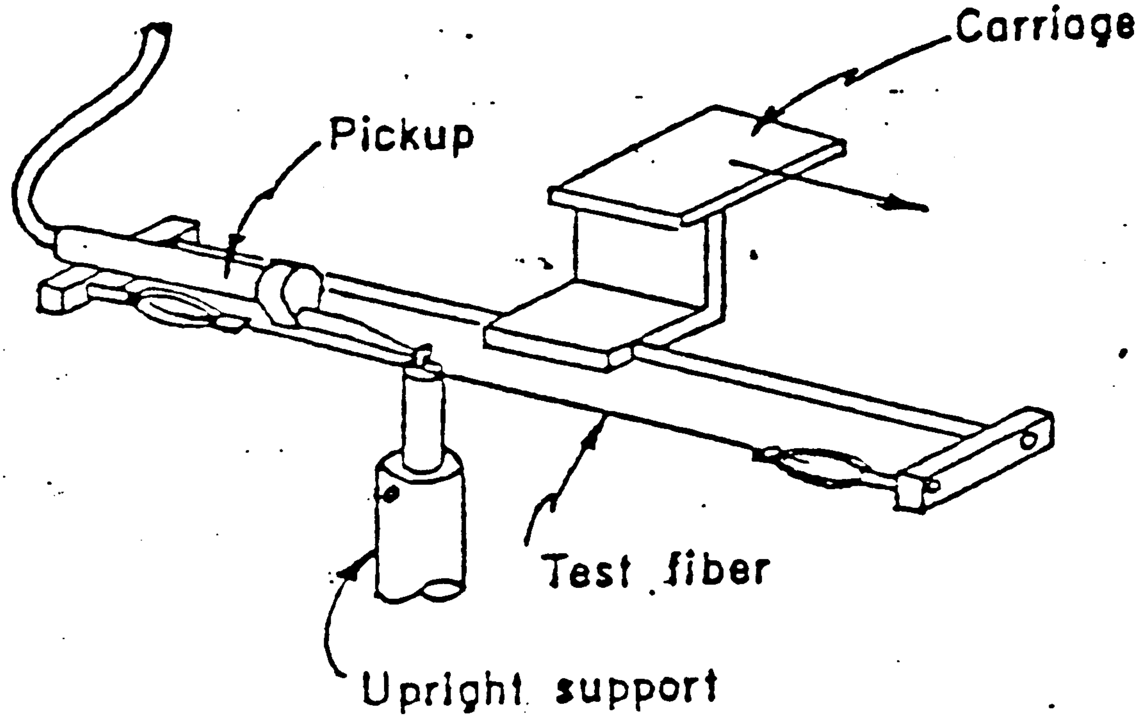

Figure 2.3: Stylus profilometer [11].

variations in the image plane of diffusely transmitting and reflecting objects. They studied the relationship between the RMS surface roughness measured by stylus profilometry and speckle contrast C, which is defined as

$$C = V/\overline{I} \qquad (2.3)$$

where V is the variance of intensity and $\overline{I}$ is the mean intensity. Speckle contrast was found to be linearly related to RMS surface roughness.

A disadvantage of speckle contrast is that it gives no information about the frequency components of surface structure. A surface can be thought of as having roughness due to surface variations with different spatial frequencies. According to the theory of Fourier analysis, a wave always can be separated into a series of sinusoid waves of different frequency. Although spatial frequency information is not available from speckle contrast measurements, the Fourier transform technique provides a means of obtaining this information.

2.4.3 NONCONTACT METHOD : FOURIER TRANSFORM

Recent years have seen great interest in surface roughness research using Fourier Transform methods. In the late 1970's, B.J.Pernick[21] developed a method to measure the surface roughness of flat objects with an optical Fourier spectrum analyzer as shown in Figure 2.4. Metallic samples were placed directly behind a square aperture and illuminated with a polarized laser beam partially reflected with a beam splitter. Light from the surface is collected with a Fourier Transform

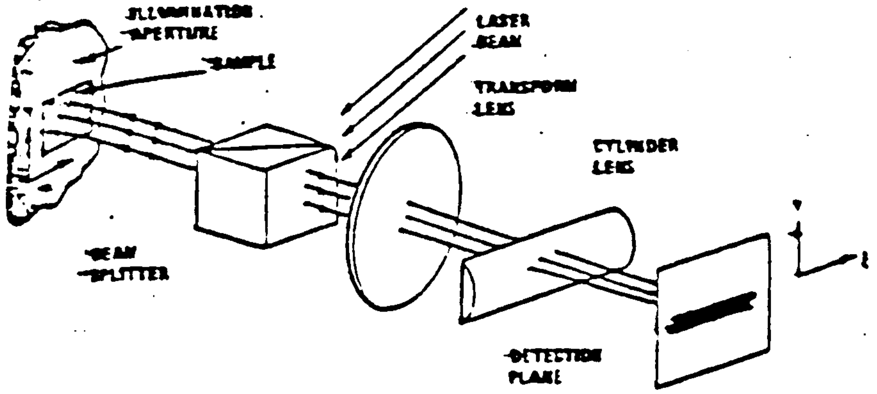

Figure 2.4: Optical system for 1-D Fourier analysis of scattered light from a rough surface developed by B.J.Pernick [21].

lens and a cylinder lens. The cylinder lens averages the signal in one dimension and forms a 1-D Fourier spectrum in a detector plane located at the common back focal plane of the transform lens and image plane of the cylinder lens. The results showed roughness height of standard templates and transform patterns to be linearly related. In addition, scattered light peak widths and surface roughness height are well represented by a linear relation over a broad range.

In 1987, Allardyce and George[22] presented both theoretical and experimental analysis using the optical Fourier spectrum analyzer shown in Figure 2.5. They showed that the far-field back scattering pattern is the Fourier Transform of the scattered object surface by comparing computer calculated transforms with optical transforms measured with their Fourier spectrum analyzer. They showed that the transform patterns can be related to roughness by 5% of the central spectrum area, the standard deviation of intensity, and specular peak intensity.

2.5 FUNDAMENTALS OF FOURIER TRANSFORMS AND FOURIER OPTICS

2.5.1 FOURIER TRANSFORMS

A mathematical tool of great utility in the analysis of frequency components is Fourier analysis. Any periodic signal can be represented by an infinite sum of weighted sinusoids called a Fourier series. The form of the Fourier series represen-

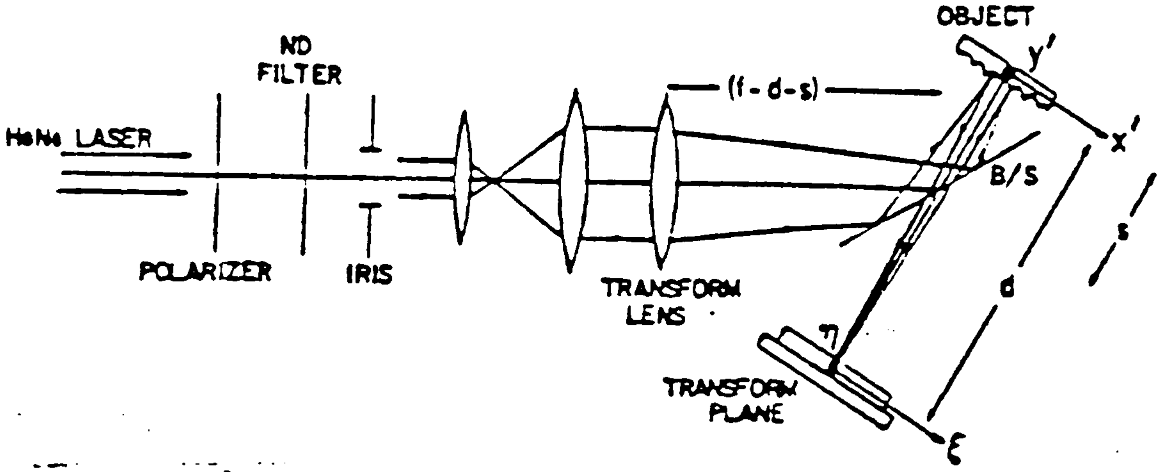

Figure 2.5: Optical system for 1-D Fourier analysis of scattered light from a rough surface developed by Allardyce and George [22].

tation of a periodic function g(x) with period,2π is

$$g(x) = \frac{a_0}{2} + \sum_{n=1}^{\infty}(a_n cosnx + b_n sinnx) \qquad (2.4)$$

where,

$$a_n = \frac{1}{\pi}\int_{-\pi}^{\pi} g(x)cosnxdx \qquad (2.5)$$

$$b_n = \frac{1}{\pi}\int_{-\pi}^{\pi} g(x)sinnxdx \qquad (2.6)$$

By expanding the convergence interval from -π to π, to-∞ to $+\infty$, one can generalize the Fourier series for periodic functions to the Fourier transform for non-periodic functions as follows:

$$\mathcal{F}[g(t)] = G(\omega) = \int_{-\infty}^{+\infty} g(t)exp(-j\omega t)dt \qquad (2.7)$$

where $\mathcal{F}$ denotes Fourier operator, $g(t)$ denotes input function in time-domain and t is time variable, $G(\omega)$ denotes Fourier transform of input function $g(t)$ in frequency-domain and $\omega = 2\pi f$ where f denotes frequency.

and the inverse transform

$$\mathcal{F}^{-1}[G(\omega)] = g(t) = \frac{1}{2\pi}\int_{-\infty}^{+\infty} G(\omega)exp(+j\omega t)d\omega \qquad (2.8)$$

where $\mathcal{F}^{-1}$ denotes inverse Fourier transform.

This Fourier transform pair can be easily extended to two-dimensions using a function g(x,y) of two variables:

$$\mathcal{F}[g] = \int\int_{-\infty}^{+\infty} g(x,y)exp[-j2\pi(ux+vy)]dxdy \qquad (2.9)$$

$$\mathcal{F}^{-1}[G] = \int\int_{-\infty}^{+\infty} G(u,v)exp[+j2\pi(ux+vy)]dudv \qquad (2.10)$$

The coordinates x and y are the "space-domain" coordinates and the coordinates u and v are the "spatial- frequency-domain" coordinates.

2.5.2 FRAUNHOFER DIFFRACTION

Diffraction may be defined as any deviation of light from straight paths not explained by reflection or refraction[23,24].

Considering the geometrical situation as Figure 2.6, if the aperture width and height are much greater than a wavelength and the observation plane is fairly close to the aperture, the image is nearly predicted by classical ray optics. On the other hand, light and dark fringes may be present on the observation plane if the light is coherent. According to the Huygens-Fresnel principle, the electromagnetic field amplitude, E, at the observation plane can be expressed as

$$E(x_0,y_0) = \int\int_{-\infty}^{+\infty} h(x_0,y_0;x_1,y_1)E(x_1,y_1)dx_1dy_1 \qquad (2.11)$$

where $E(x_0,y_0)$ denotes electromagnetic field at observation plane, $E(x_1,y_1)$ denotes electromagnetic field at aperture plane, and $h(x_0,y_0;x_1,y_1)$ denotes the impulse response of the system which is defined as

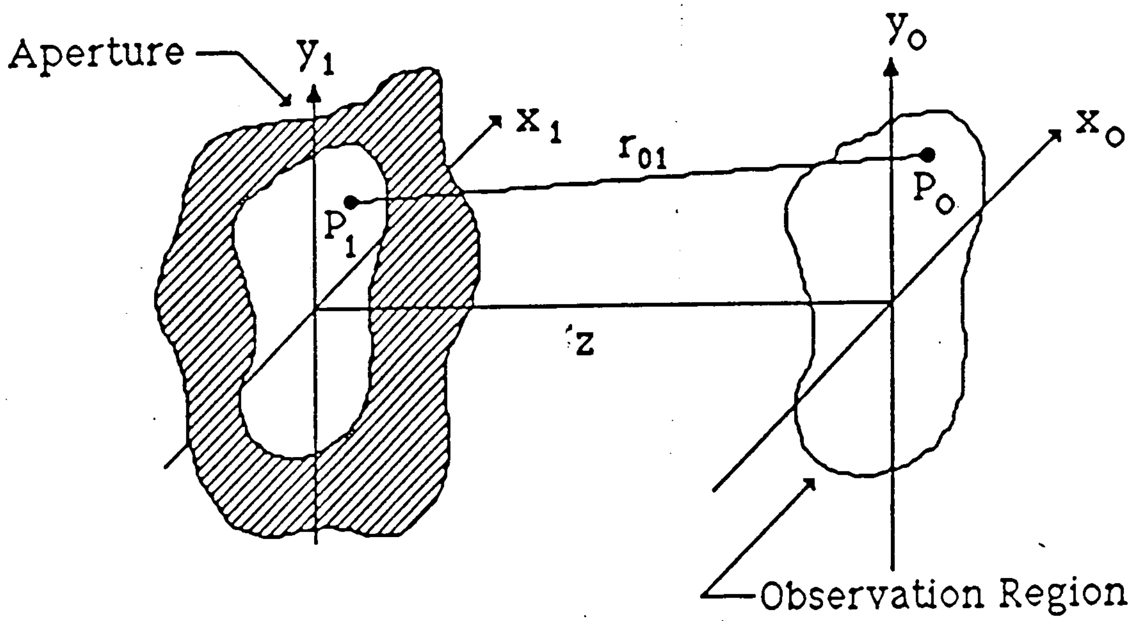

Figure 2.6: Diffraction geometry [23].

$$h(x_0, y_0; x_1, y_1) = \frac{1}{j\lambda}\frac{exp(jkr_{01})}{r_{01}}cos(\overline{n}, \overline{r_{01}}) \qquad (2.12)$$

where k is termed the wave number and is given by $k = 2\pi/\lambda$, λ is the wave length, r_{01} is the distance between point P_1 and P_0 as shown in Figure 2.6, $cos(\overline{n}, \overline{r_{01}})$ is termed obliquity factor.

If the Fresnel approximation was used[23], the integral describing Fresnel diffraction can be written as

$$E(x_0, y_0) = \frac{exp(jkz)}{j\lambda z}exp\{j\frac{k}{2z}[x_0^2 + y_0^2]\} \int\int_{-\infty}^{+\infty} E(x_1, y_1)exp\{j\frac{k}{2z}[x_1^2 + y_1^2]\}$$

$$exp\{-j\frac{2\pi}{\lambda z}[x_0x_1 + y_0y_1]\}dx_1dy_1 \qquad (2.13)$$

If the distance between the aperture and observation plane, Z, is much greater than the aperture itself,

$$Z \gg k(x_1^2 + y_1^2)/2 \qquad (2.14)$$

where k is the wave number, for any x_1 and y_1 in the aperture, then the phase factor involving x_1 and y_1 inside the integral is approximately unity over the whole aperture and the Fresnel integral reduces to the Fraunhofer integral

$$E(x_0, y_0) = \frac{exp(jkz)}{j\lambda z}exp\{j\frac{k}{2z}[x_0^2 + y_0^2]\}$$

$$\int\int_{-\infty}^{+\infty} E(x_1, y_1)exp\{-j\frac{2\pi}{\lambda z}[x_0x_1 + y_0y_1]\}dx_1dy_1 \qquad (2.15)$$

Notice that it is exactly the Fourier integral except for some extra multiplicative phase and amplitude factors outside the integral sign, where the spatial frequencies are

$$u = x_0/\lambda z \qquad \textit{and} \qquad v = y_0/\lambda z \qquad (2.16)$$

The power of the illumination is not dependent on the phase and therefore the Fraunhofer illumination is a scaled version of the squared magnitude of the Fourier transform.

CHAPTER III

COMPUTER SIMULATION STUDIES

3.1 INTRODUCTION

In Chapter II, diffraction theory was reviewed and it was noted that the far-field Fraunhofer diffraction pattern is the two-dimensional Fourier transform of the transmittance from scattering object. It was also noted that this relationship could be similarly applied to back scattering if the transmittance function is replaced by a reflectance function. Since Fourier transformations can be performed easily on digital computers, information about expected scattering patterns can be obtained if the input is the reflectance of a surface structure. Relationships between structural variables such as fiber diameter or cross- sectional shape and scattering patterns can be found by digital Fourier transforms.

The assumptions associated with these computations are that there are no multireflections on fiber surfaces and the amplitudes of illumination is not changed by reflection.

The following topics are discussed in this chapter:

1. Surface structures and interpretation of their scattering patterns.

2. The influence of RMS asperity height and slope distribution on the scattering pattern.

3. The influence of fiber diameter and cross-sectional shape on the scattering

pattern.

3.2 ROUGH SURFACE GENERATION

Fiber models were generated by adding random numbers to the fiber cross-sectional shape functions along the fiber axis.

3.2.1 FIBER CROSS-SECTIONAL SHAPE FUNCTION

In order to investigate the influence of different fiber cross-sectional shapes on scattering, three cross- sectional shapes were generated. These are referred to as rectangular, circular and triangular and are illustrated in Figure 3.1.

For a rectangular fiber cross-section, the cross- sectional shape function is given by

$$Z = \begin{cases} a & y_1 < y < y_2 \\ 0 & \text{otherwise} \end{cases} \qquad (3.1)$$

where a denotes the minor rectangle diameter.

For a circular cross section, the cross-sectional shape function is given by

$$Z = \begin{cases} \sqrt{r^2 - y^2} & y < r \\ 0 & y > r \end{cases} \qquad (3.2)$$

where r denotes the fiber radius.

For a triangular cross section, the cross-sectional shape function is given by

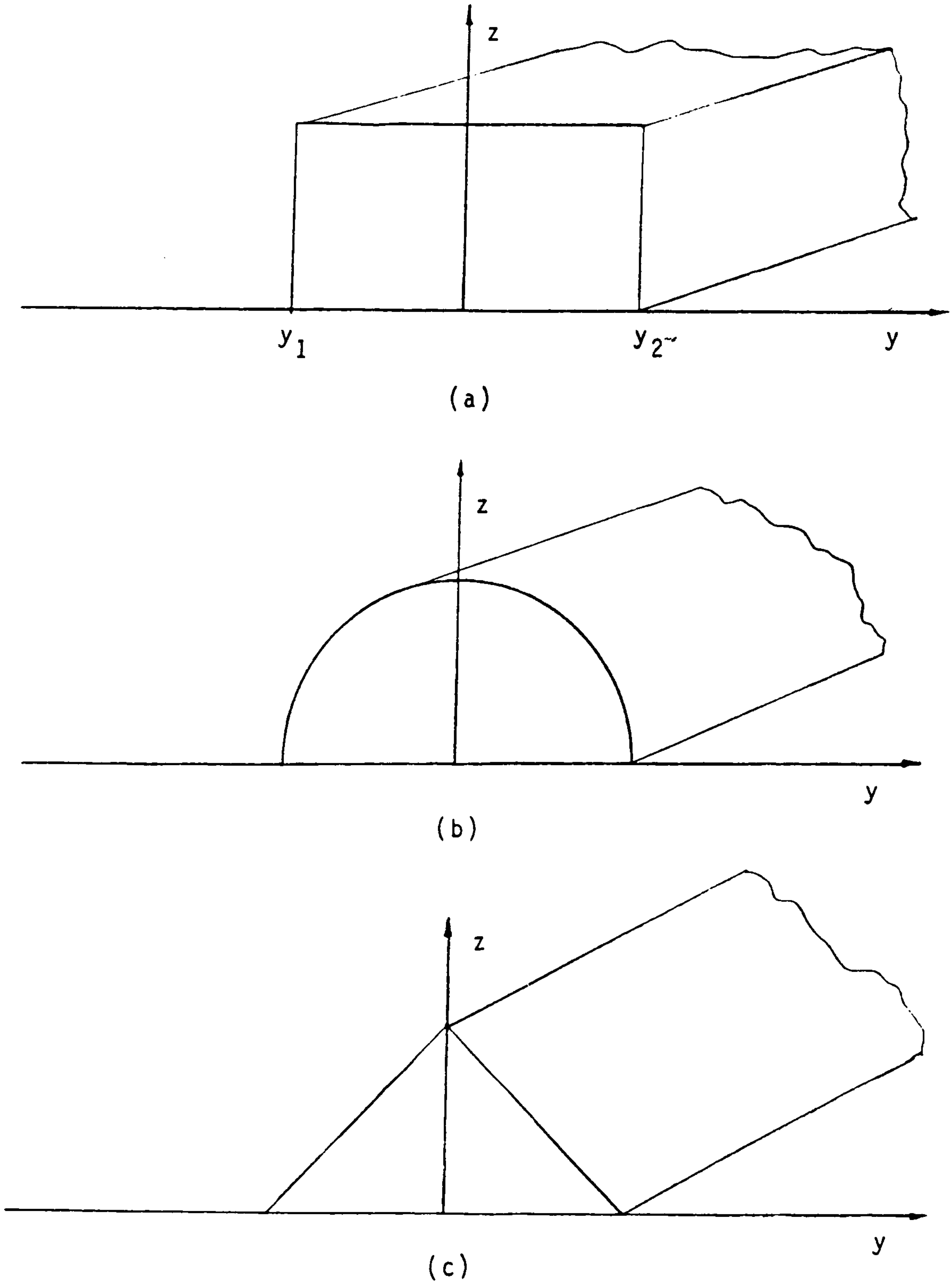

Figure 3.1: Fiber cross-sectional shapes for a) rectangular, b) circular and c) triangular fiber models.

$$Z = \begin{cases} ky + b & y < 0 \\ -ky + b & y > 0 \end{cases} \qquad (3.3)$$

where k denotes dz/dy and b denotes the height.

3.2.2 SURFACE ASPERITY SHAPE GENERATION

In studies of surface roughness, not only does the RMS height of the surface asperities affect the scattering pattern, but the slope distribution of surface asperities affects it as well. A better understanding of a surface and its scattering pattern may be obtained by generating surfaces using different asperity shapes such as square, triangular, $sine^2$ wave, or random.

Figure 3.2 illustrates four fiber surfaces in one dimension along the fiber axis with different asperity shapes and each with a RMS surface roughness equal to 0.15. The spacing and height of random square, triangular and $sine^2$ wave asperity shapes are randomly distributed.

From the Central limit theorem, we know that the sum of random variable R_i will be close to a Gaussian distribution when N is large enough. That is

$$\sum_{i=1}^{N} R_i \sim \mathcal{N}(\sum_{i=1}^{N} \mu_i, \sum_{i=1}^{N} \sigma_i^2) \qquad (3.4)$$

where N denotes the number of random data, $\mathcal{N}$ denotes Gaussian distribution, R_i denotes ith random data, μ_i denotes ith mean and σ_i^2 denotes ith variance.

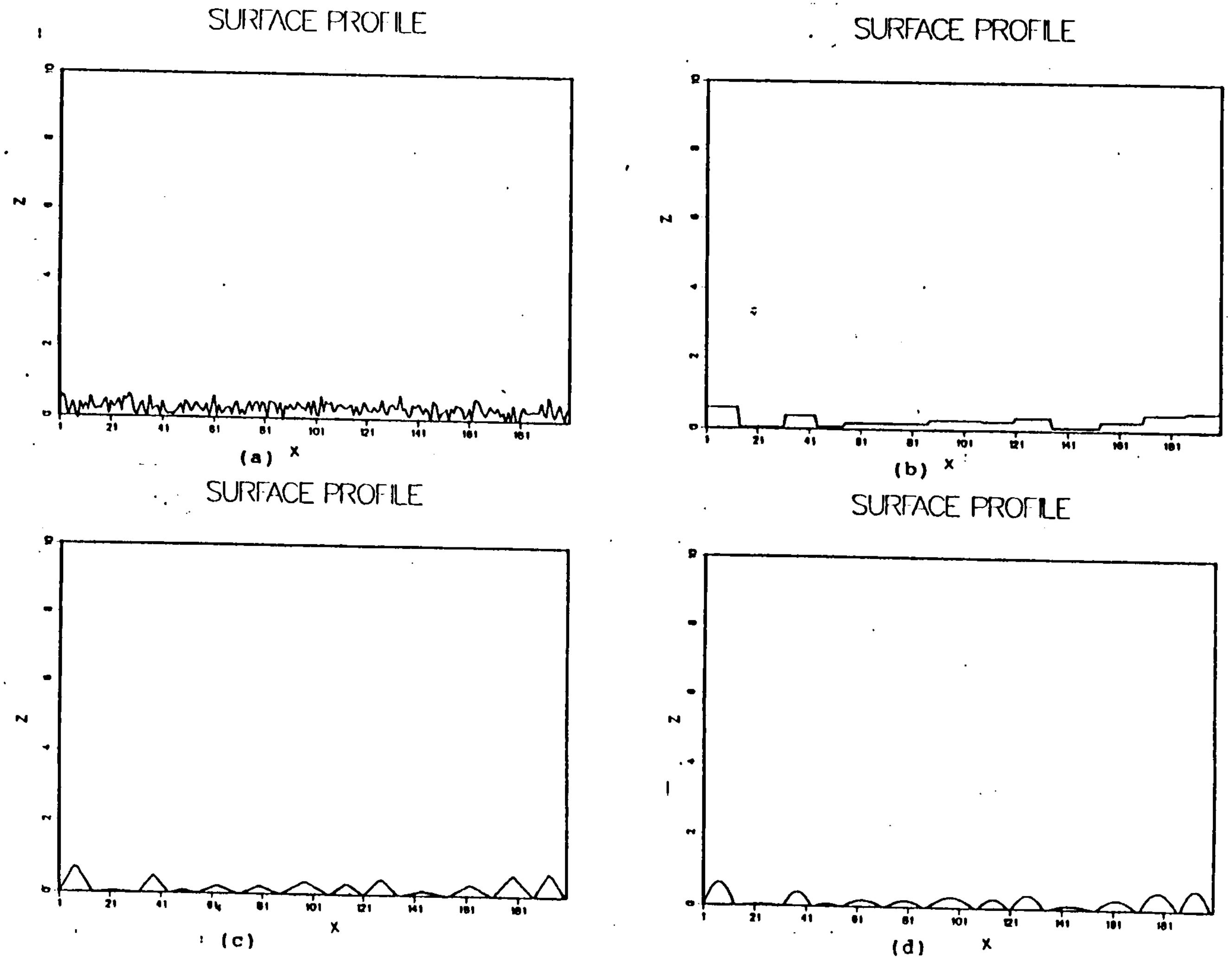

Figure 3.2: One dimensional surface profiles along the fiber axis for a) random, b) square, c) triangular, d) $sine^2$ wave asperity shape models.

It has been shown that a good approximation can be obtained for N as small as $N = 12$ [25].

Eq.(3.5) gives points Z_i' of a Gaussian distribution with mean μ and standard deviation σ, where $N = 12$.

$$Z_i' = \mu + \sigma(\sum_{i=1}^{12} R_i - 6.0) \qquad (3.5)$$

Fiber surface models are generated by adding asperity shape data to each fiber cross-sectional shape function. Surface heights of a fiber, h_i, are given by

$$h_i = Z_i + Z_i'/C \qquad (3.6)$$

where Z_i is determined by the fiber cross-sectional shape function and Z_i' is a data point from a Gaussian distribution of either random, square, triangular or $sine^2$ shape functions. C is a variable used to control RMS surface roughness. Figure 3.3 illustrates four fiber models each with a circular cross-sectional shape and with the same RMS surface roughness but with different asperity shape functions.

3.3 DERIVATION OF REFLECTANCE FROM FIBER SURFACE

The phase of incident light is changed when it encounters a rough surface. Referring to Figure 3.4, reflectance can be derived as follows[22]. Assuming the optical axis lies along the fiber diameter, an expression for the phase perturbation

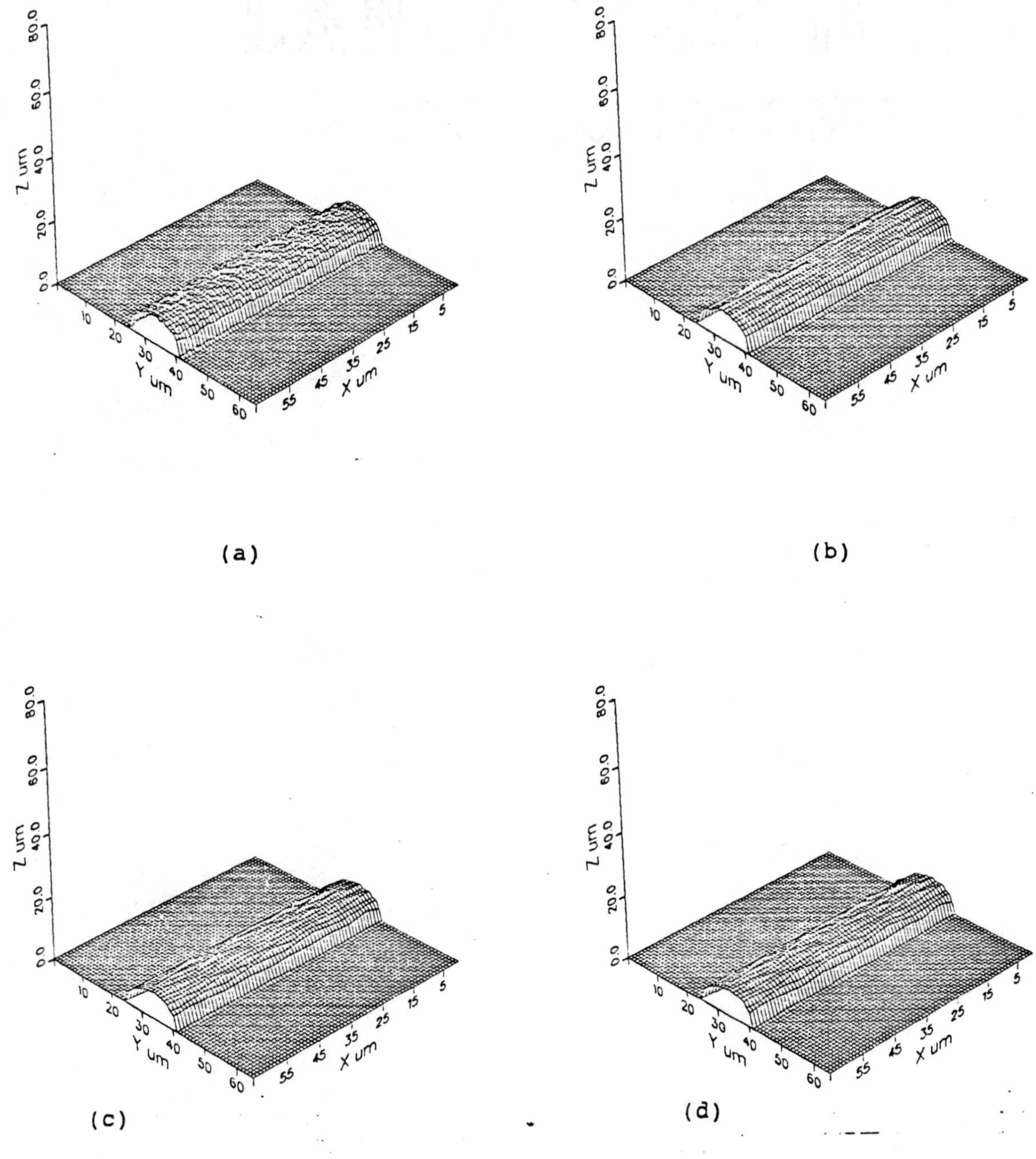

Figure 3.3: Fiber models with circular cross-sectional shapes and , a) random asperity shapes, b) square asperity shapes, c) triangular asperity shapes, d) $sine^2$ wave asperity shapes.

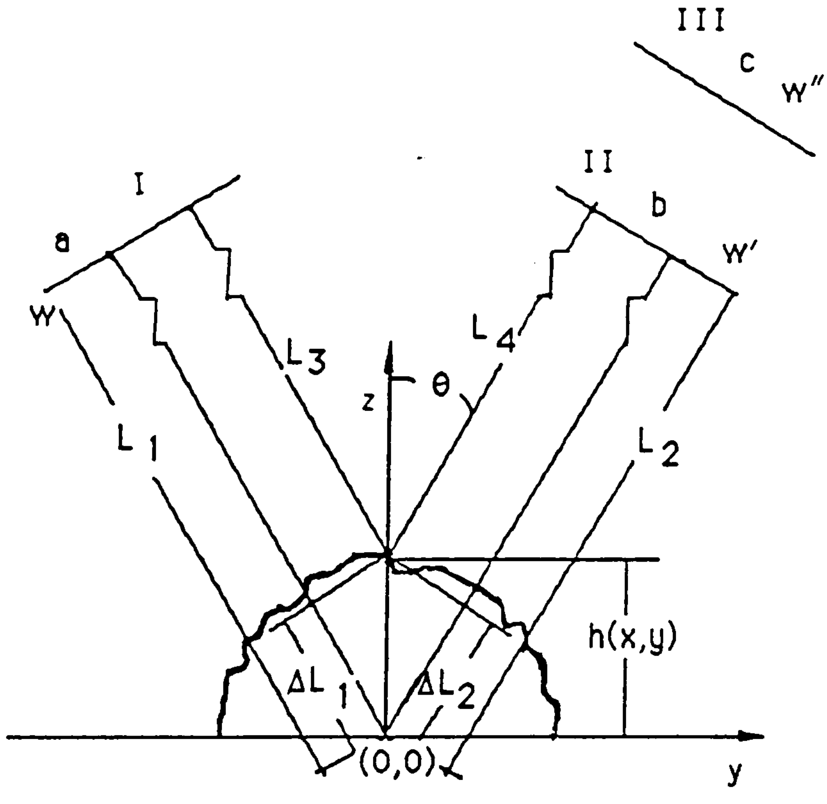

Figure 3.4: Rough surface representation.

of an incident wave, w, caused by a fiber surface which is represented by a height function, h(x,y) can be derived[22].

At an arbitrary position in the (x,y) plane such as (0,0), the zero-roughness phase retardation is determined by the distance $L_1 + L_2$, this sum being independent of the position (x,y) in the plane. The surface roughness point, h(x,y), changes the path length to $L_3 + L_4$. To determine the reflectance, R(x,y), the differences in path length, $\Delta L_1 + \Delta L_2$, are needed. We write the actual path $L_3 + L_4$ as

$$L_3 + L_4 = (L_1 + L_2) - (\Delta L_1 + \Delta L_2) \qquad (3.7)$$

where

$$\Delta L_1 + \Delta L_2 = 2h(x,y)cos\theta \qquad (3.8)$$

Now, for the phase term $exp(i\omega t)$ using Eqs. (3.7) and (3.8) and dropping unessential constant phase delays, we define the reflectance function R(x,y) by

$$R(x,y) = exp[j2kh(x,y)cos\theta] \qquad (3.9)$$

in which $k = 2\pi/\lambda$ is defined as the wave number, and λ is the wavelength of the illumination.

Since equation (3.9) gives us an expression for the perturbed phase front W' at II (space domain), we can write the output scalar component of the field $E(x_0, y_0)$

at the observation plane III (frequency domain), if it is located at a distance great enough to meet the requirement of Fraunhofer diffraction. The paraxial form is given by[22]

$$E(x_0, y_0) = A \int\int_{-\infty}^{+\infty} R(x,y) exp[-j2\pi(x_0 x + y_0 y)/(\lambda z)] dx dy \qquad (3.10)$$

in which A is a constant, R(x,y) is given by Eq.(3.9), and z is the distance between the fiber surface and the observation plane.

Substitutions of $u = x_0/(\lambda z)$ and $v = y_0/(\lambda z)$ into Eq.(3.10), considering the case of normal illumination, where $\theta = 0$, and substituting Eq.(3.9) for R(x,y), the result becomes

$$E(u, v) = A \int\int_{-\infty}^{+\infty} exp[j2kh(x,y)] exp[-j2\pi(ux + vy)] dx dy \qquad (3.11)$$

Refering to Eq.(2.9), it can be seen that the g(x,y) is given by $exp[j2kh(x,y)]$ in Eq.(3.11), so this expression shows that the scattering pattern can be calculated by Fourier transform of the exponential height function.

3.4 DISCRETE FOURIER TRANSFORM AND FFT ALGORITHM

Continuous Fourier transform theory can be modified to allow digital computation using a discrete Fourier transform. The discrete Fourier transform pair is defined as

$$F(u, v) = \frac{1}{MN} \sum_{x=0}^{M-1} \sum_{y=0}^{N-1} f(x,y) exp[-j2\pi(ux/M + vy/N)] \qquad (3.16)$$

for u=0,1,2,...,M-1, v=0,1,2,...,N-1.

$$f(x,y) = \sum_{u=0}^{M-1} \sum_{v=0}^{N-1} F(u,v)exp[j2\pi(ux/M + vy/N)] \qquad (3.17)$$

for x=0,1,2,...,M-1, and y=0,1,2,...,N-1.

The number of complex multiplications and additions required to implement Eq. (3.16) is proportional to N^2. In order to reduce the number of computations involved in a Fourier transform, a fast Fourier transform (FFT) algorithm [27] is used to compute the discrete Fourier transform. The number of multiplications and addition operations can be made proportional to $Nlog_2N$. The reduction from N^2 to $Nlog_2N$ represents significant saving in computational effort particularly when N is relatively large. The FFT algorithm used is based on the so-called "successive doubling" method by dividing the original expression into two parts successively.

3.5 THE METHODS TO ANALYZE BACK SCATTERING PATTERN

Several researchers have studied techniques for characterizing the surface roughness of metallic materials. B.J.Parnick[21] suggested that the Gaussion width of the scattering spectrum was a good measure of surface roughness. K.J.Allardyce[22] used measurements based on the standard deviation of the scattering spectrum, specular peak(zero frequency) intensity and 5% of the central spectrum area. Although their work indicated that there were linear relationships between these spectral measurements and surface roughness of the samples they examined, their measurements are quite different.

The Gaussion width is the band width of the spectrum and it only shows how many frequency components comprise the surface waviness. A large standard deviation of a scattering spectrum only means it has large variations in frequency components and thus is not directly related to surface roughness. Specular peak intensity is directly related to surface roughness, but it also is affected by fiber diameter if fibers are examined. Luster ratio was developed by Nicherson[9] to evaluate cotton fiber luster. In his method, scattered light intensities were measured at 0^o and 45^o and the ratio of these two intensities was called luster ratio. It is notable that the use of luster ratio minimized the influence of fiber diameter on roughness measurements. However, luster ratio values are based on only two specific reflections (0^o and 45^o) and these are measured in a near- field. On the other hand, far-field scattering falls into the special-frequency domain and we can obtain spatial frequency information from the spectrum. A perfectly smooth surface will show high intensity located only at zero frequency (for 0^o incidence of light source). On the other hand, a fiber surface which is not smooth will exhibit reduced zero frequency intensity and the intensity at other frequencies will be increased according to the nature of the surface roughness. Therefore, the integral of all frequency components with respect to zero frequency will give a measure of fiber surface roughness without the influence of diameter. Roughness Coefficient is thus defined as

$$RC = I_t/I_0 \qquad (3.18)$$

where RC is the roughness coefficient, I_0 is the intensity at zero frequency and I_t represents the total intensities scattered at other frequencies. The I_t term will be zero for a perfectly smooth surface so the RC value is equal to zero and the greater I_t becomes, the rougher will be the fiber surface.

3.6 DESIGN OF COMPUTER PROGRAM

A program "Laser Back Scattering.FOR" was written to compute the theoretical scattering pattern from fiber models. A flowchart of this program appears in Figure 3.5. First, a fiber cross-sectional shape and surface asperity shape were selected. The reflectance function is computed for the model using Eq.(3.9) and then, a two-dimensional Fourier transform of this function was performed using a FFT[27] modified to operate in two-dimensions as explained belows in Eq.(3.19). Finally, the theoretical back scattering pattern was plotted as intensity verses spatial frequency and RC is computed from the scattering pattern. The main program is quite straightforward. The important parameters are selected through the dialogue method.

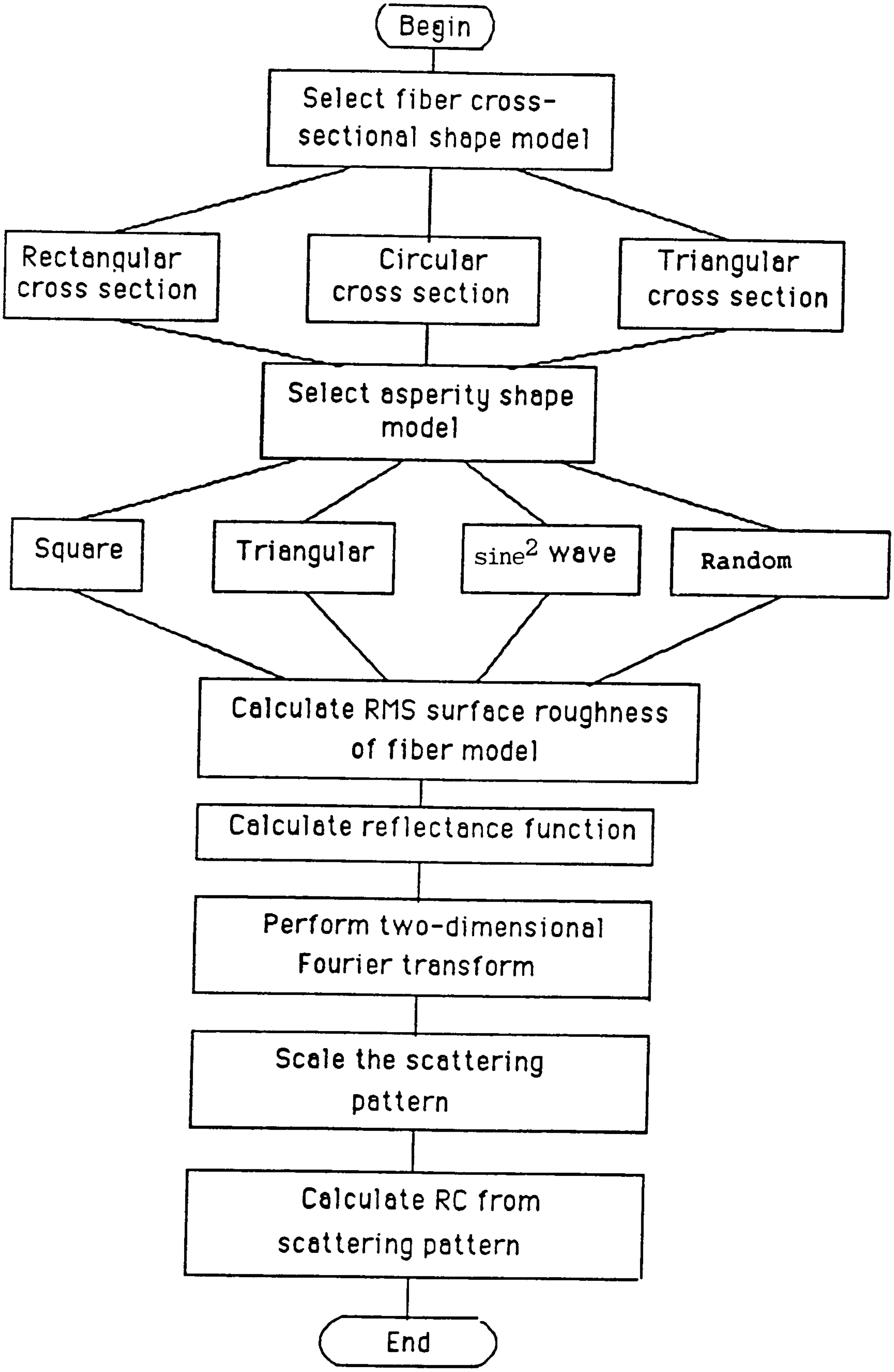

Figure 3.5: Flowchart of the program.

The two-dimensional Fourier transform is performed in the subroutine, TFFT, using the principle of separability and an FFT algorithm[27]. The principal advantage of the separability property is that F(u,v) can be obtained in two steps by successive applications of the one-dimensional Fourier transform as follows:

$$F(u,v) = \frac{1}{N}\sum_{x=0}^{N-1} F(x,v)exp[-j2\pi ux/N] \qquad (3.19)$$

where

$$F(x,v) = N[\frac{1}{N}\sum_{y=0}^{N-1} f(x,y)exp[-j2\pi vy/N]] \qquad (3.20)$$

For each value of x, the expression inside the brackets is a one-dimensional transform with frequency values v=0,1,2,...,N-1. Therefore, the two-dimensional function F(x,v) is obtained by taking a transform along each row of f(x,y) and multiplying the result by N. The desired result, F(u,v), is then obtained by taking a transform along each column of F(x,v).

The subroutine "CENTER" centers the Fourier spectrum. The symmetry property shows that the magnitude of the transform is centered about the origin and the periodicity property indicates that F(u,v) has a period of length N. Since the discrete Fourier transform has been formulated for values of u and v in the interval [0,N-1], the result of this formulation yields two back to back periods in this interval. To display only one full period, the origin of the transform is moved to the point u=N/2 and v=N/2. This is accomplished by multiplying f(x,y) by

$(-1)^{(x+y)}$ prior to taking the transform.

A subroutine "SCL" was written to display the scattering pattern with different scales. Either linear or logarithmic scaling my be selected by the parameter ISCL. The SCL subroutine also can adjust the data to the maximum dynamic range by the parameter IAUTO.

The subroutine "RC" was used to calculate a parameter called the roughness coefficient, RC, from the scattering pattern. The RC value was determined by the ratio I_t/I_0, where It is the sum of all the data above or below zero spatial frequency in the u direction and Io is the sum of all the data at zero frequency.

3.7 RESULTS AND DISCUSSION

The basic question addressed in this section is whether or not actual fiber back scattering patterns obtained under conditions satisfying the Fraunhofer requirement are similar to the "scattering patterns" computed by Fourier transformation of the reflectance from a fiber model resembling the actual fibers.

Figure 3.6 (a) is a scattering pattern recorded photographically on polaroid film from a polyethylene fiber of circular cross-sectional shape of about 40 um diameter suspended vertically relative to the film as shown. Typically the (0,0) point is located approximately 8mm to the left middle of each photograph as conventionally displayed. Figure 3.6 (b) is the theoretical scattering pattern computed

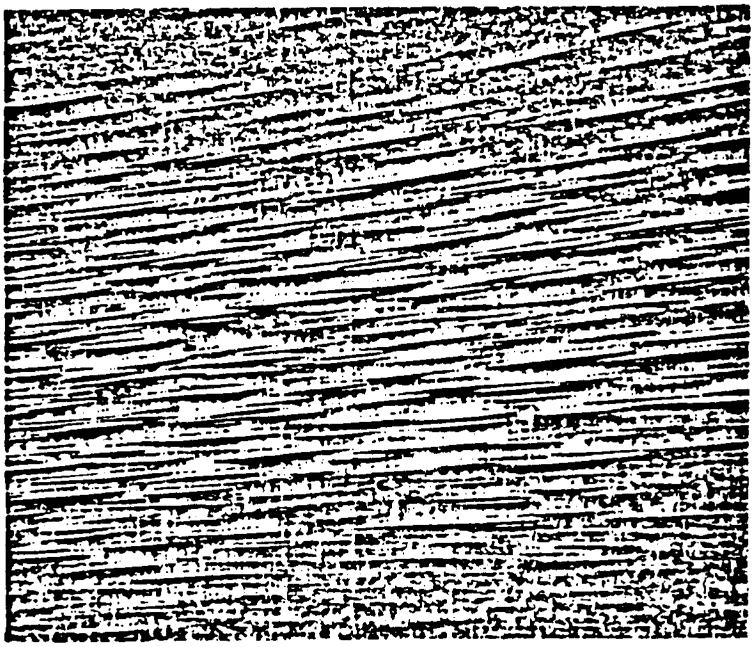

(a) Actual scattering pattern from a polyethylene fiber of circular cross-sectional shape of diameter=40 um.

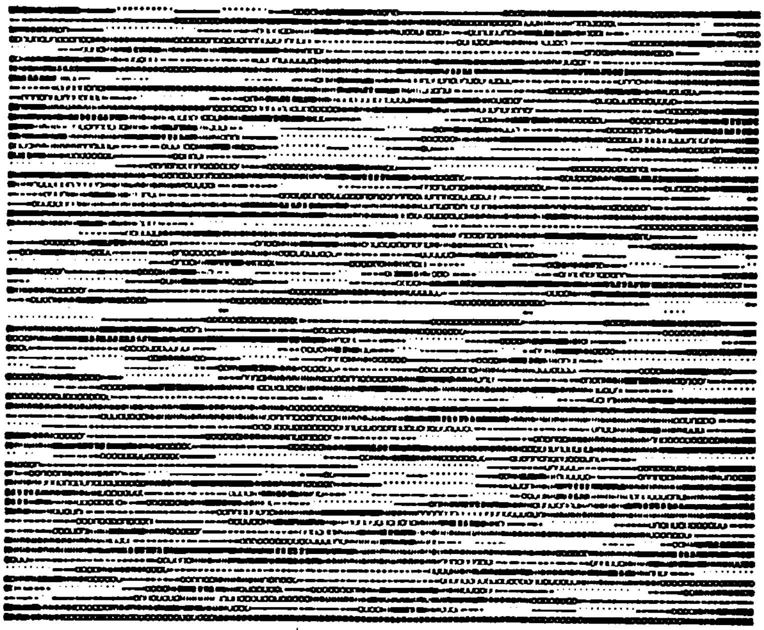

(b) Fourier transform (theoretical scattering pattern) of a fiber model having a circular cross-sectional shape, random asperity shape, RMS asperity height=0.15 um, and fiber diameter=40 um.

Figure 3.6: Actual scattering pattern and theoretical scattering pattern, a) actual scattering pattern, b) theoretical scattering pattern.

for a fiber model having a circular fiber cross-sectional shape of 40 um diameter with a random asperity shape and RMS asperity height =0.15 um. The (0,0) point is located in the center of the graph. Although the image quality of Fig. 3.6 (b) is not good because it was displayed on a line printer by overstriking characters to give a desired gray level and the image was only composed of 64 by 64 pixels, similarity between the actual measured and computed patterns is evident.

In order to improve image quality, fiber models and their transforms were plotted three-dimensionally using a software program called "TECHPLOT" developed at Tennessee Tech University. Figure 3.7 shows typical plots of a fiber model and its Fourier transform represented as scattering intensity vs spatial frequency. The scattering intensity at a spatial frequency (u, v) is set equal to the squared magnitude of the Fourier transforms.

$$I(u,v) = [Re^2(E(u,v)) + Im^2(E(u,v))] \qquad (3.22)$$

where E(u,v) is the fast Fourier transform value at a spatial frequency u, v. The spatial frequency values calculated by the FFT are defined by

$$u = n/(N\Delta x) \qquad n = -N/2, ..., 0, ... + N/2 \qquad (3.23)$$

$$v = n/(N\Delta y) \qquad n = -N/2, ..., 0, ... + N/2 \qquad (3.24)$$

where N=256 is the total number of sample points, Δx is the sample spacing in the x direction equal to the total interval length divided by the number of

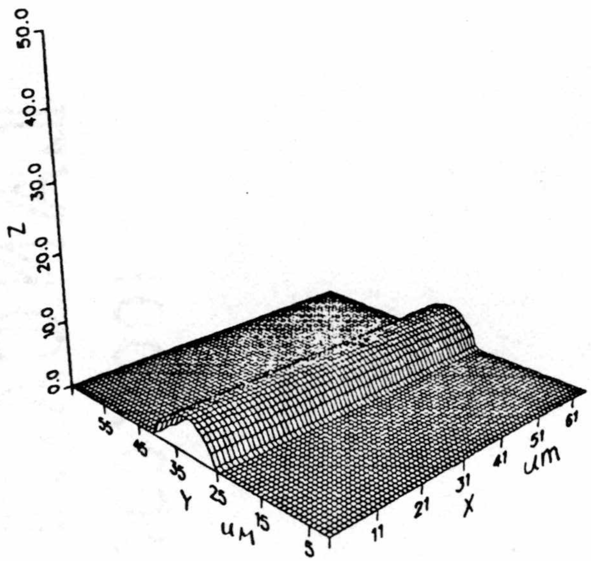

(a)

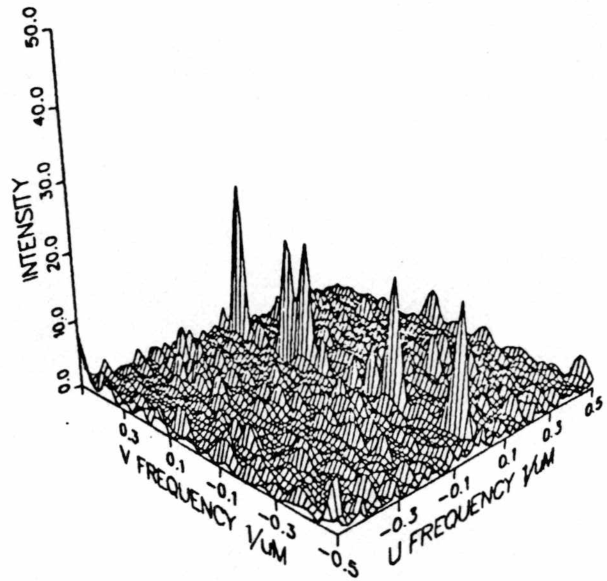

(b)

Figure 3.7: Fiber model and its theoretical scattering pattern, a) fiber model: circular fiber cross-sectional shape , fiber diameter=16 μm, random asperity shape, RMS asperity height=0.09 μm, b) scattering pattern computed from the model: RC=14.87.

sample points N, and Δy is defined similarly but in the y direction. The images of fiber models were restricted to 256x256 pixels. If the sampling intervals Δx and Δy equal $1\mu m$ (total sampled length along fiber axis is $256\mu m$), Δu, Δv is $1/256\mu m^{-1}$ and the maximum frequencies calculated by the FFT are equal to $0.5\mu m^{-1}$. The maximum frequencies attainable decrease as the sampling intervals increase while the number of sample points remains constant. For example, if the sampling intervals are $4\mu m$ (total sampled length along fiber axis is $1024\mu m$), the maximum frequency will be $0.125\mu m^{-1}$ and Δu, Δv are equal to $1/1024\mu m^{-1}$.

The scattered intensity at the origin of the u axis, I(0,v), is the specular reflection term and corresponds to the smooth part of the surface along the x fiber direction. I(0,v) data contains information about the fiber diameter and cross-sectional shape. Any data points above or below this line are due to fiber surface roughness. Intensities along v directions in spatial-frequency domain are mainly from surface waviness along y directions in space domain, whereas intensities along the u directions in spatial- frequency domain are mainly from surface waviness along the x directions in space domain (fiber axis). These can be explained better using two-dimensional plots. Taking x directions (fiber axis) for example, if the fiber surface is smooth, Fig. 3.8 (a), the intensity at u=0 in spatial- frequency domain will quite high, Fig. 3.8 (b). In the extreme smooth case, there will be an impulse located at u=0 and it will tend to be infinity. On the other hand, if

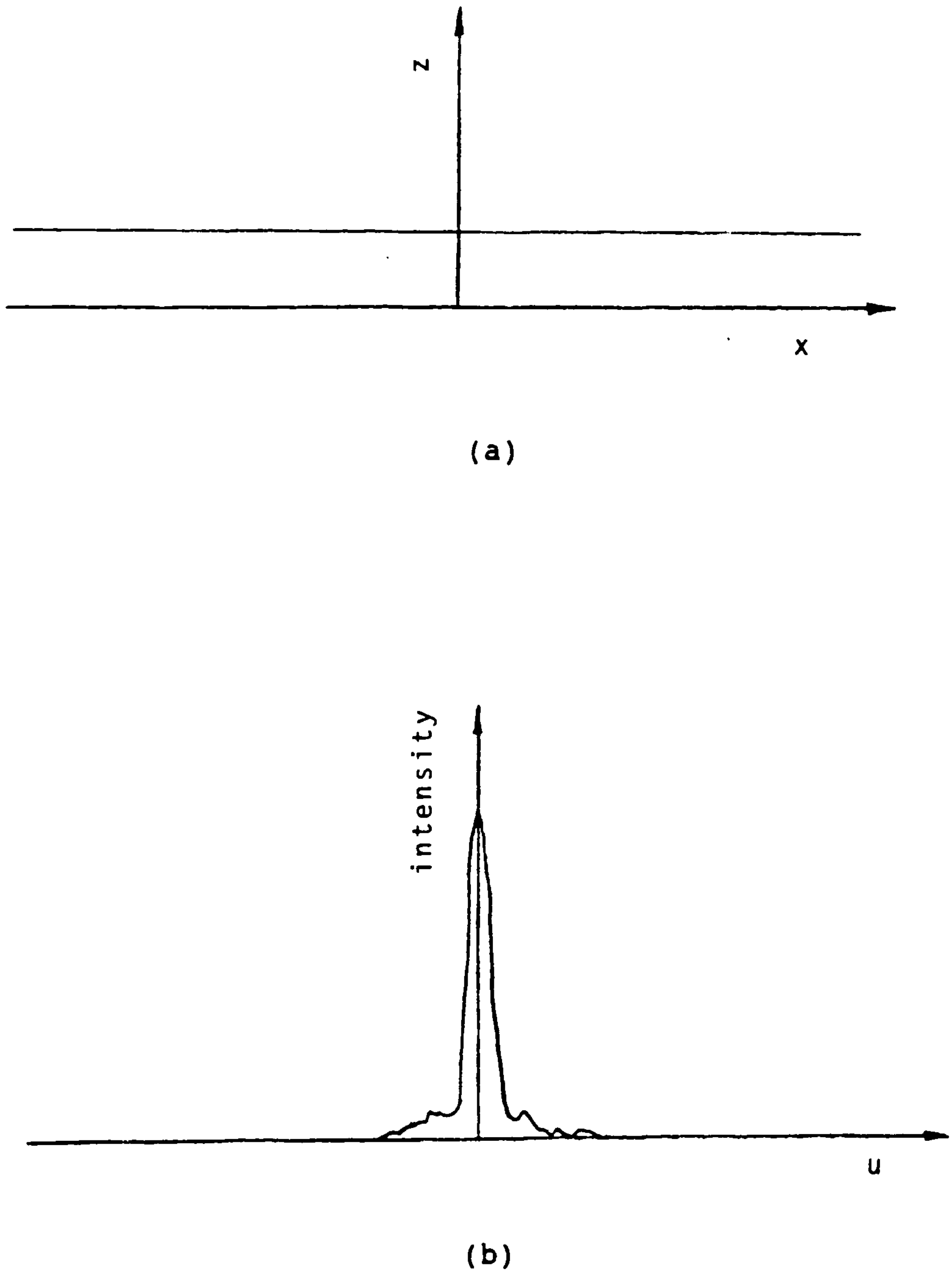

Figure 3.8: Smooth fiber surface and its theoretical scattering pattern, a) fiber surface and b) theoretical scattering pattern.

surface is relatively rough, Fig. 3.9 (a), the zero frequency intensity will decrease and be more spread out, Fig. 3.9 (b).

For the purpose of investigating the theoretical influence of RMS asperity height on scattering patterns, four fiber models were used having the same fiber diameter, circular fiber cross-sectional shape and random asperity shape but having different RMS asperity height. RMS height ranged from quite smooth (RMS=0.02) to rough (RMS=0.16). Figures 3.10 and 3.11 show the four fiber models and their corresponding Fourier transforms, respectively.

Figure 3.10 (a) is a smooth fiber (RMS=0.02) and it's Fourier transform pattern is quite simple as shown in figure 3.11 (a) and is characterized by RC=0.10. There is no theoretical scatter above or below the u=0 spatial frequency and scatter at u=0 is an impulse along the v direction. This means that the fiber surface along its x axis (fiber axis) is smooth since a constant and an impulse is a Fourier transform pair.

Figure 3.10 (b) represents a slightly rough fiber surface with RMS asperity height of 0.05. The theoretical scattering pattern from the fiber model in Figure 3.11 (b) shows that scattered intensity at u=0 is reduced compared to Figure 3.11 (a) and many scattering humps have emerged from uv plane although their intensity is small. The RC value associated with this scatter was computed to be 1.78 which indicates that the fiber surface is slightly more rough than that of

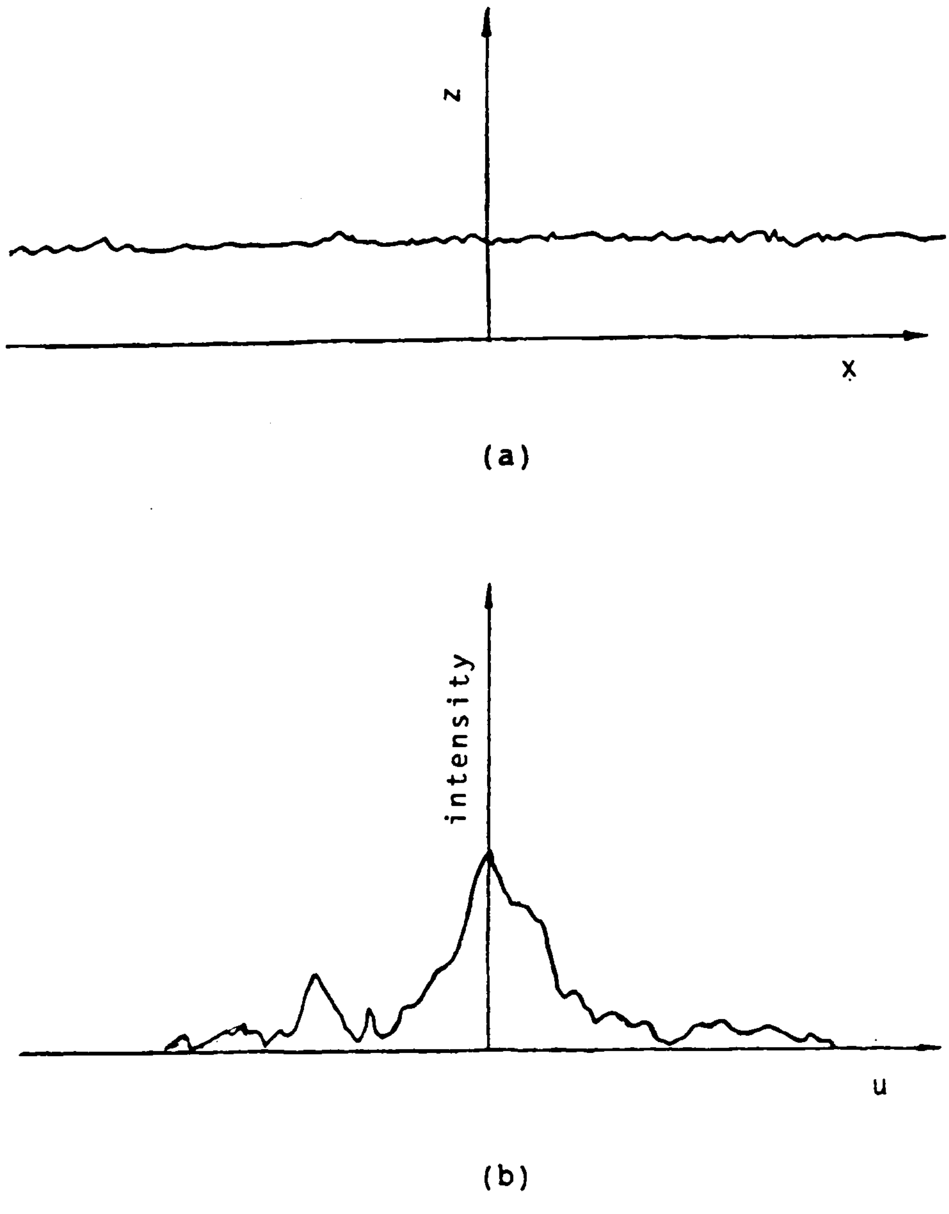

Figure 3.9: Rough fiber surface and its theoretical scattering pattern, a) fiber surface and b) theoretical scattering pattern.

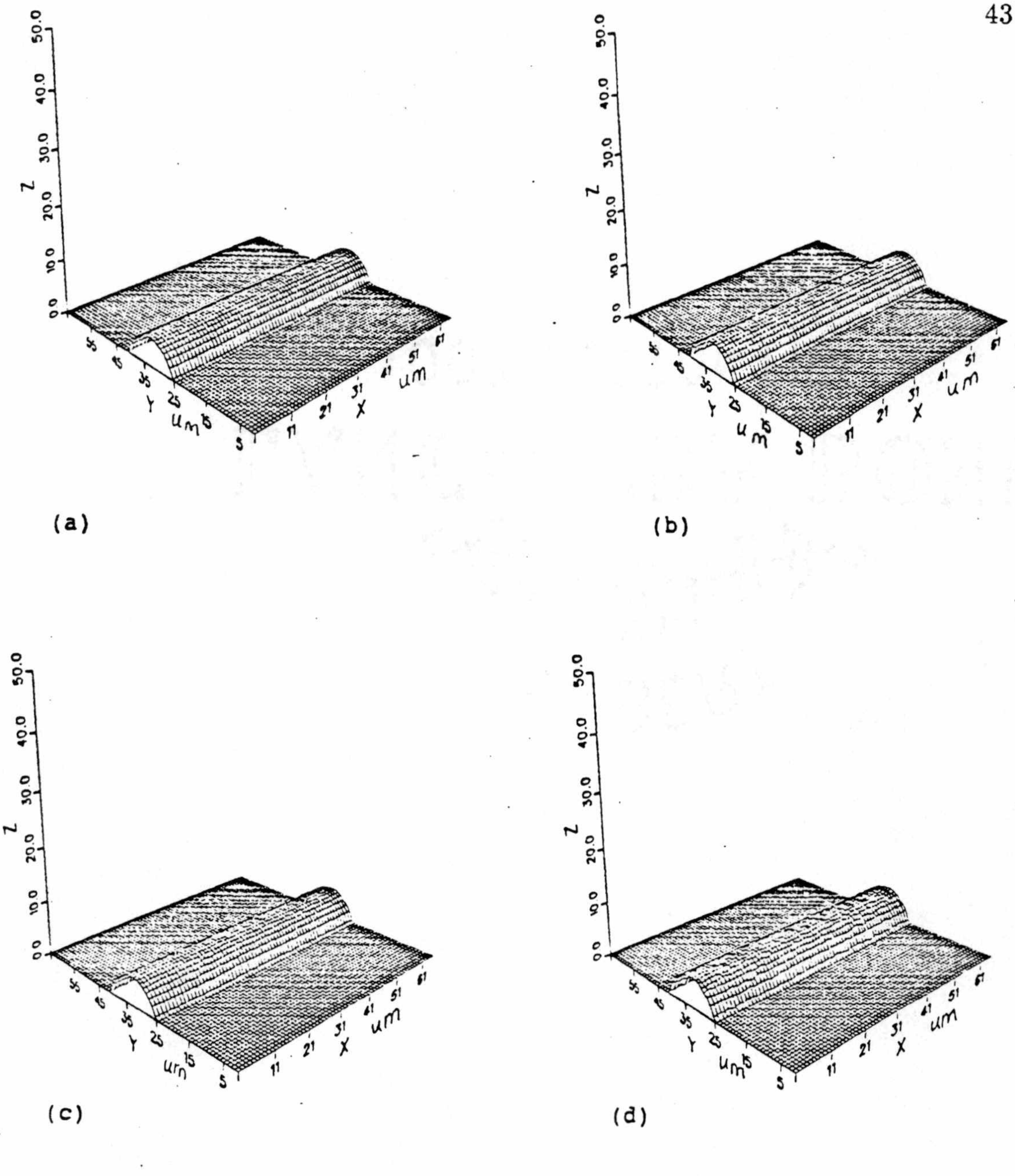

Figure 3.10: Fiber models having the same fiber diameters, circular cross-sectional shapes and random asperity shape but different RMS asperity height, a) RMS=0.02 μm, b) RMS=0.05 μm, c) RMS=0.08 μm, d) RMS=0.16 μm.

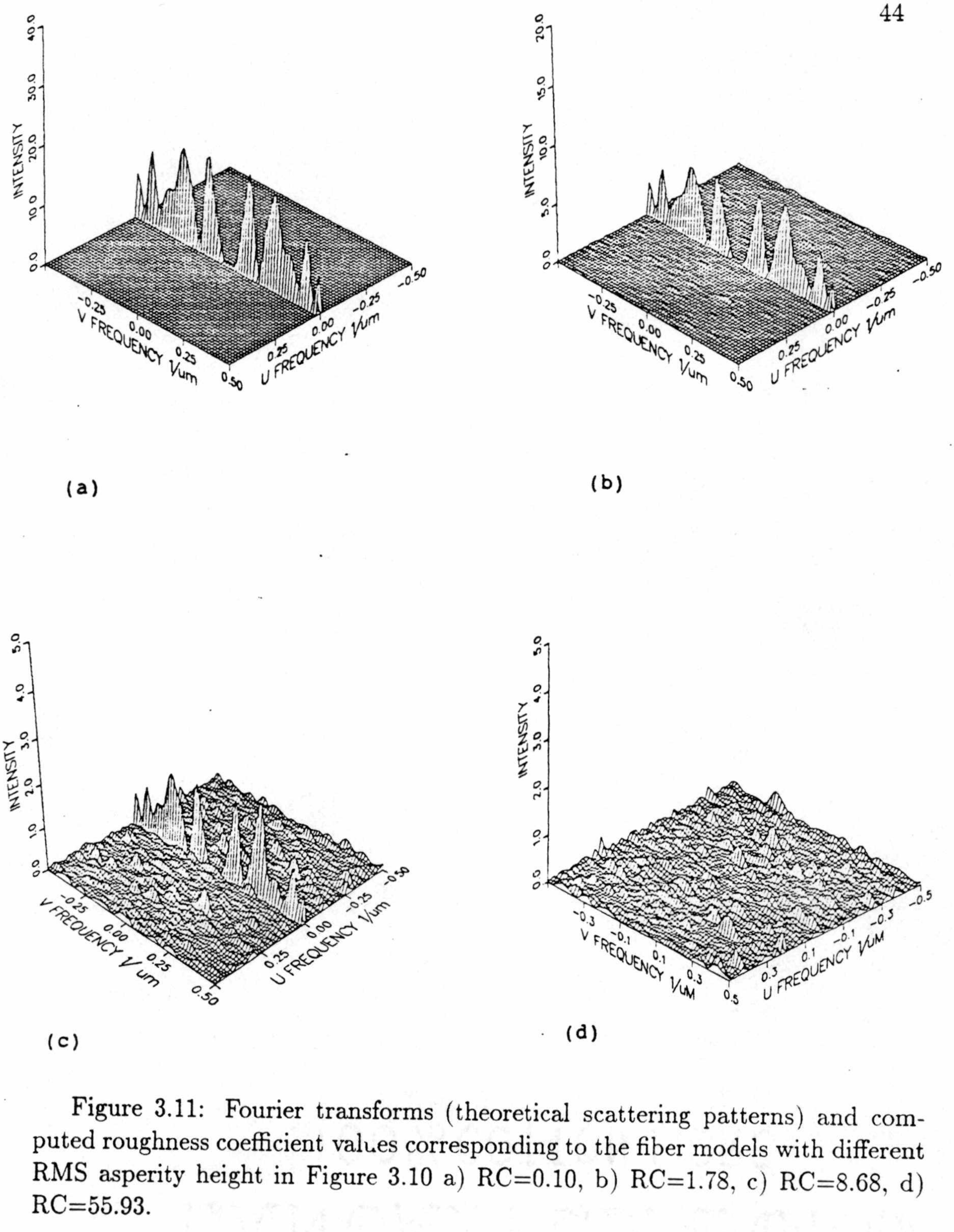

Figure 3.11: Fourier transforms (theoretical scattering patterns) and computed roughness coefficient values corresponding to the fiber models with different RMS asperity height in Figure 3.10 a) RC=0.10, b) RC=1.78, c) RC=8.68, d) RC=55.93.

3.10(a).

Figure 3.10 (c) and (d) represent further increases in RMS asperity height to 0.08 and 0.16. The Fourier transforms illustrated in Figure 3.11 (c) and (d) show a further reduction in scattered intensity at u=0 and a further increase in the number and intensity of scattered humps throughout the scattering region. The RC values for these two fibers were computed to be 8.68 and 55.93. In conclusion, these results show that theoretical back scattering patterns from fibers are greatly influenced by the height of asperities on the fiber surfaces.

In order to investigate the influence of asperity shape on theoretical scattering patterns, four fiber models were used which have the fiber diameters of 16 um, circular fiber cross-sectional shapes, and RMS asperity heights of 0.15, but varied in asperity shape. Asperity shapes included random, square, triangular and $sine^2$ wave shapes as shown previously in Figure 3.3. Figure 3.12 shows the theoretical scattering patterns for these fibers. Despite the same RMS asperity height for each of the four fiber surfaces, the theoretical scattering patterns differ greatly. These differences can be easily seen qualitatively and are expressed quantitatively in the RC values computed from each of the scattering patterns.

Referring to Figure 3.12, one can see a difference in the intensity of scattered light appearing at higher u frequencies as well as in the u=0 frequency region. The square asperity shape exhibited the least high frequency scatter and the greatest

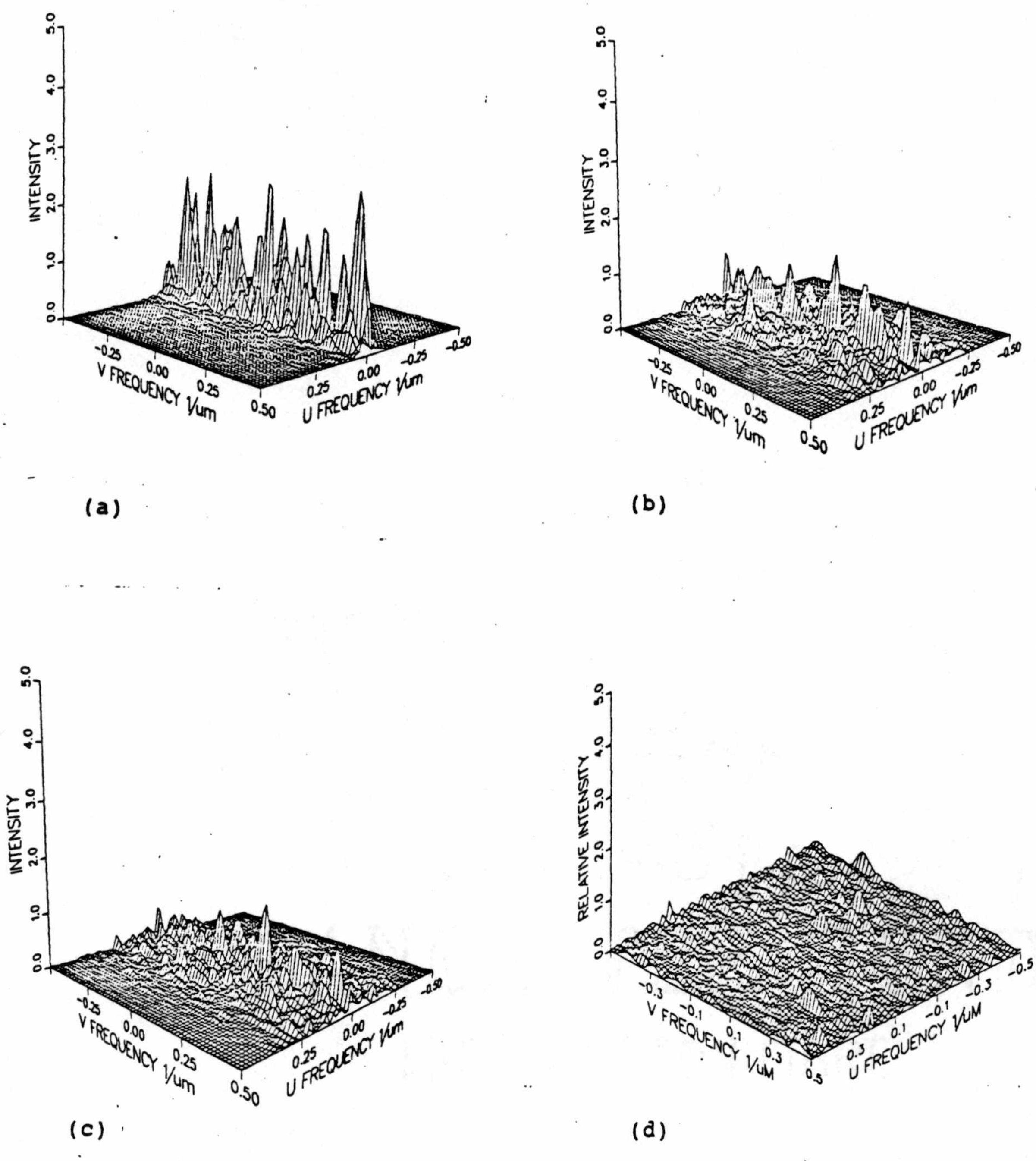

Figure 3.12: Fourier transforms (theroretical scattering patterns) and computed RC values for fiber models with fiber diameters=16 μm, circular fiber cross-sectional shapes, RMS asperity height=0.15 μm, but different asperity shapes: a) square, RC=3.89, b) triangular, RC=11.36, c) $sine^2$, RC=12.93, d) random, RC=57.93.

amount of zero frequency scatter. On the other hand, the random asperity shape exhibited the most high frequency scatter and least zero frequency scatter. These difference can be explained qualitatively by examining the asperity shapes in Figure 3.2. The square shaped asperities are composed entirely of flat tops, whereas the randomly shaped asperities have little flat top surface but have a large amount steeply sloped side surface which would scatter light away from the zero frequency region. The triangular and $sine^2$ wave shaped asperities can be seen to be intermediate between these two extremes. RC values computed from these theoretical scattering patterns range from 3.89 to 57.93 and thus reflect the differences in scattering observed in the patterns. In conclusion, these results show that theoretical back scattering patterns from fibers are greatly influenced by the shape of asperities on the fiber surface.

In the beginning of this section, we pointed out that scattering at the u=0 frequency provides information about fiber diameter. In order to investigate this phenomenon further we used modeling studies again to show how the scattering pattern changes with fiber diameter changes.

Figure 3.13 shows fiber models with the same circular fiber cross-sectional shape, random asperity shape and RMS asperity height=0.08 but with different fiber diameters. The diameter of the fiber in figure 3.13 (a) is $12\mu m$ whereas that of (b) is $32\mu m$. The corresponding Fourier transforms of these fibers are shown in

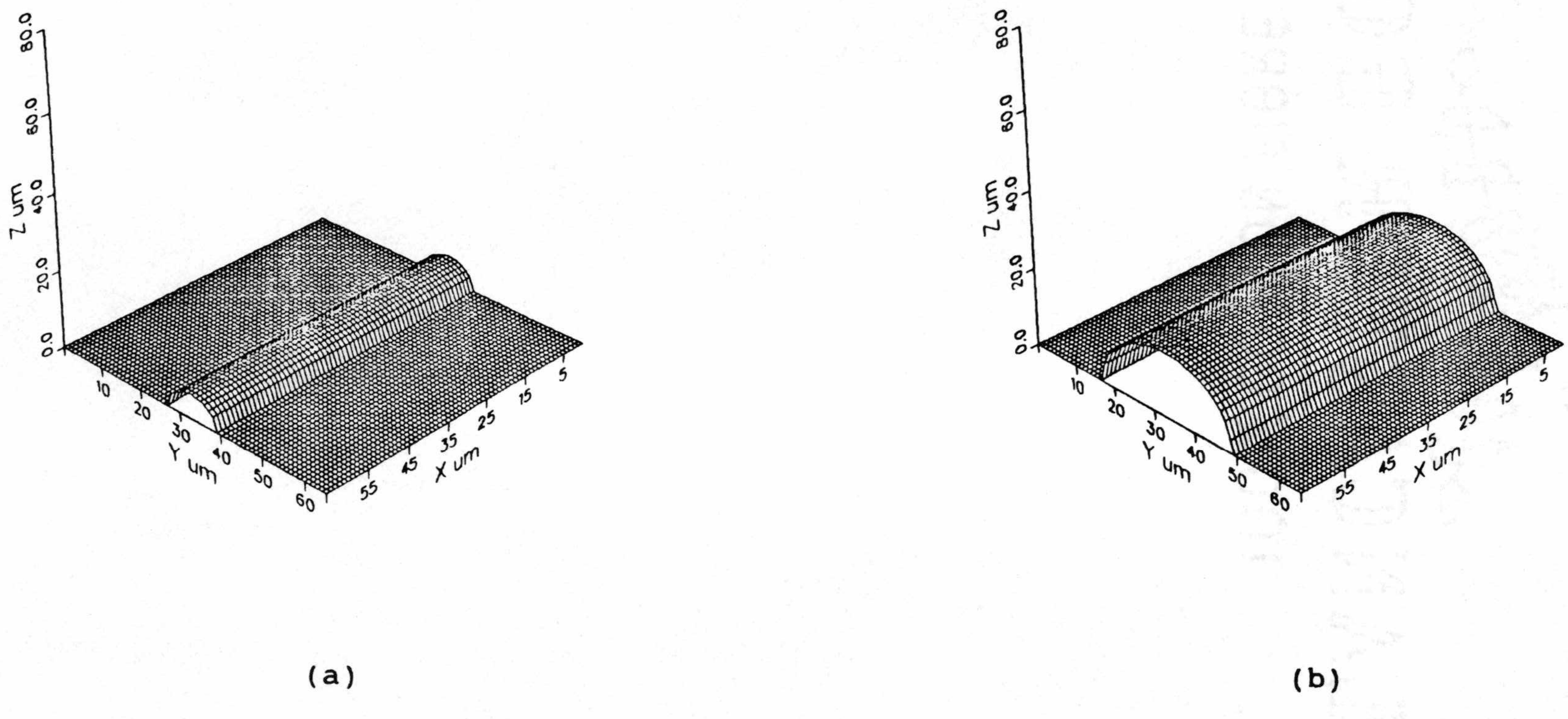

Figure 3.13: Fiber models with circular fiber cross-sectional shape, random asperity shape and RMS asperity height=0.08 μm but with different fiber diameters, a) d=12 μm, b) d=32 μm.

Figure 3.14. Because the space domain and spatial-frequency domain are inversely related, it can be seen in Figure 3.14 that the peaks at the spatial frequency u=0 move closer to the spatial frequency origin, (0,0), as the fiber diameter increased. Similar results were obtained for fibers of triangular cross- sectional shape, as shown in Figures 3.15 and 3.16, where increasing the fiber diameter shifted peaks at u=0 to lower spatial frequencies. One may conclude from this data that is should be possible to determine the diameter of fibers from back scattering measurements at the u=0 spatial frequency.

Roughness coefficient values were computed from the theoretical scattering patterns shown in Figures 3.14 and 3.16. Although RC values computed for the circular cross- sectional shaped fibers in Figure 3.14 (8.97 vs 8.48) were only slightly affected by fiber diameter differences, RC values for the triangular shaped fiber in Figure 3.16 (2.52 vs 4.97) are significantly affected by fiber diameter differences. Since space and spatial-frequency domains are inversely related, the number of peaks at the u=0 spatial frequency included in a detection plane of constant area would be a function of fiber diameter. That is, values of Io, the sum of all data at u=0 frequency, would generally be expected to be different for fibers of different diameters and the ratio $RC = I_t/I_o$ might be expected to be affected. The overall effect of fiber diameters on RC values is difficult to predict since changes in I_t values may be compensated by changes in I_o values.

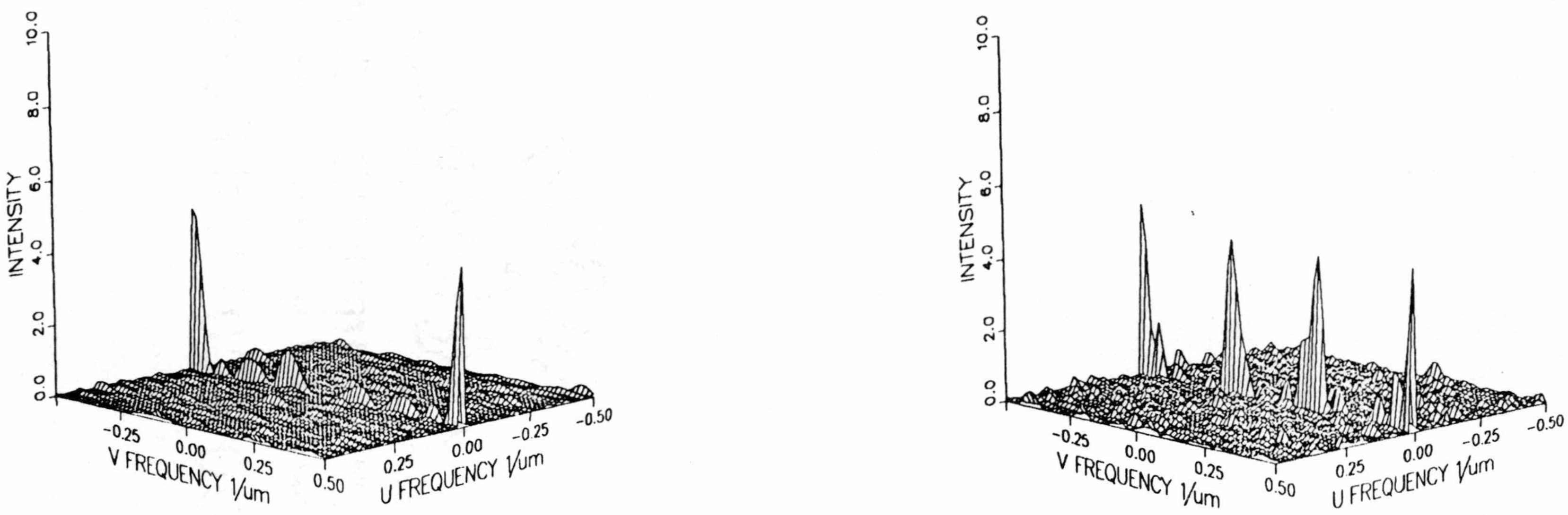

(a) (b)

Figure 3.14: Fourier transforms (theoretical scattering patterns) and computed RC values for the fiber models with different diameters in Figure 3.13, a) RC=8.97, b) RC=8.48.

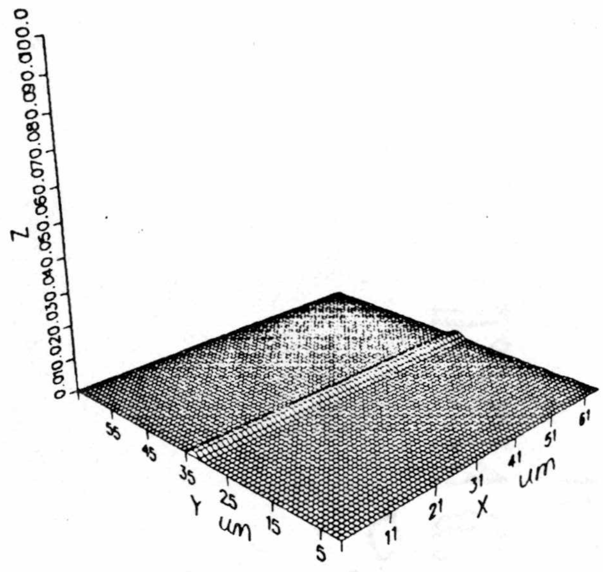

(a)

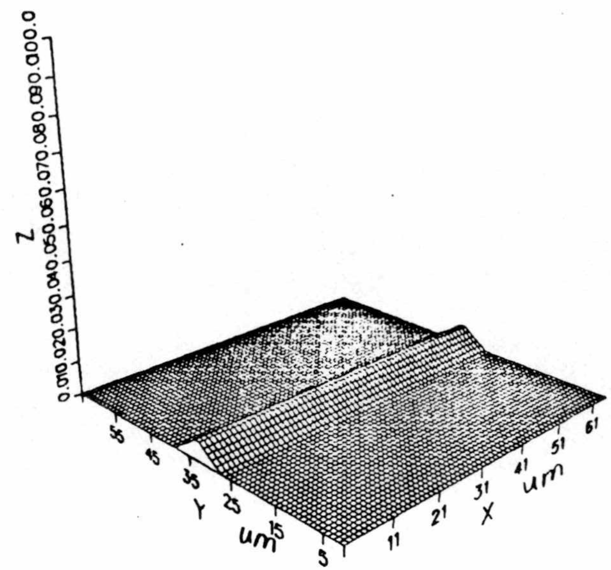

(b)

Figure 3.15: Fiber models with triangular fiber cross-sectional shape, random asperity shape and RMS asperity height=0.08 μm but with different fiber diameters, a) side length is 4 μm, b) side length is 12 μm.

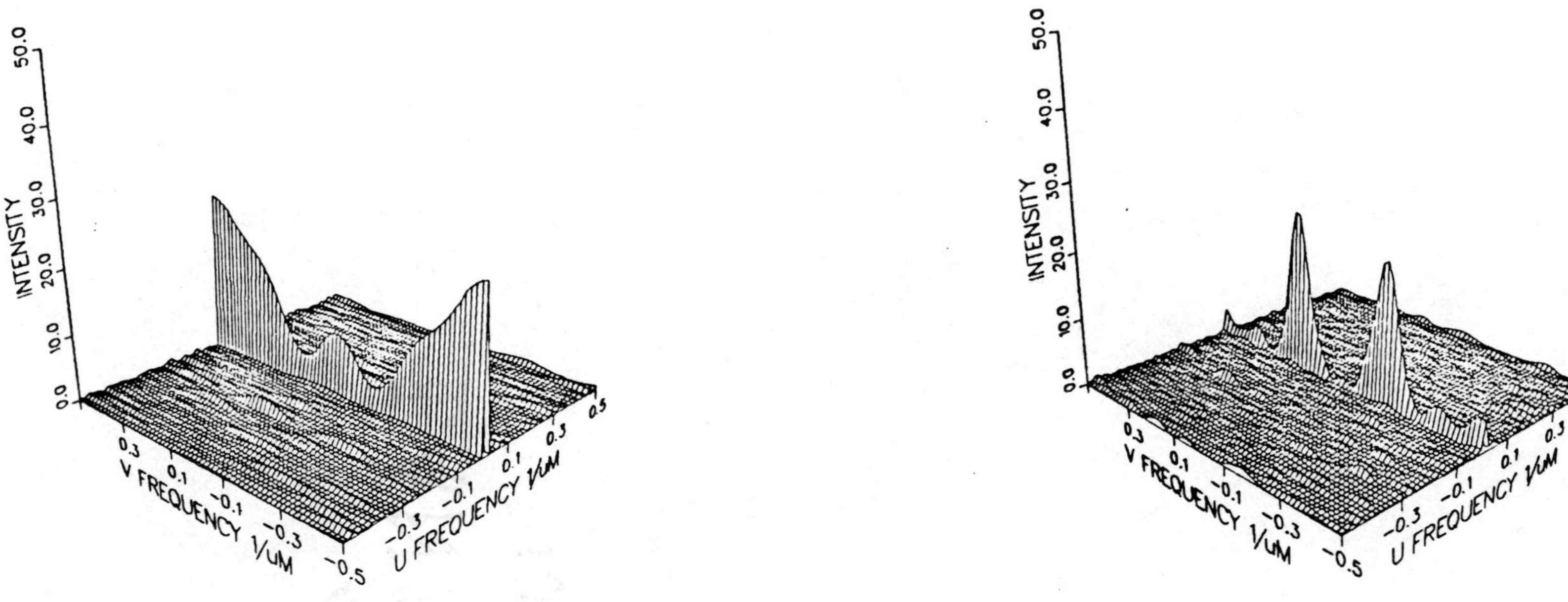

(a) (b)

Figure 3.16: Fourier transforms (theoretical scattering patterns) and computed RC values for the fiber models with different diameters in Figure 3.15, a) RC=2.52, b) RC=4.97.

To investigate the effect of fiber diameter on Roughness coefficient further, fibers were modeled with circular cross-sectional shape random asperity shape and RMS asperity height=0.08 um but with different diameters. After computing RC values from theoretical scattering patterns from each fiber, the results were plotted in figure 3.17. The plot shows that there is little long term dependance of the RC value on fiber diameters in the range of diameters examined. Figure 3.16 shows a similar plot for fibers of triangular cross-sectional shape. This plot shows that the spacing between two main peaks reduces as the fiber diameter increases.

Next, the effect of fiber cross-sectional shape on roughness coefficient values from fibers with the same RMS asperity height was examined. Since the spectrum in the u direction scatter largely contains surface information along the fiber axis direction whereas v direction scatter largely contains information about fiber diameter and cross section, we must compare scattering patterns in the v direction. Figures 3.18 to figure 3.20 show three models with the same fiber diameter,asperity shape and RMS asperity height but different cross-sectional shape. Theoretical scattering patterns and RC values computed from these scattering patterns also are provided in these Figures.

Comparing the RC values for the three models, one can find that fiber cross-sectional shape may affects RC values even though the RMS asperity height is the same. This might be explained by the limited area on which we compute RC ratio.

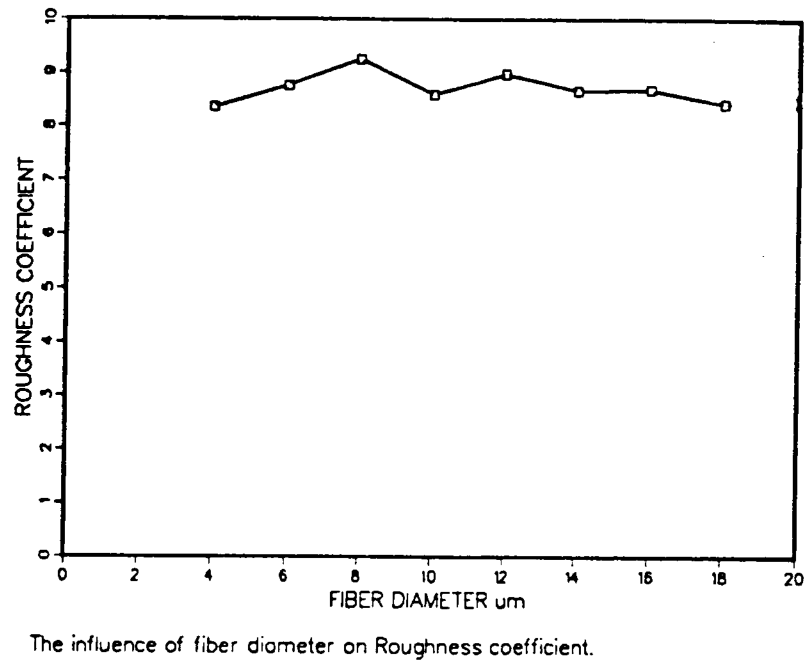

Figure 3.17: Roughness coefficients computed for fibers with circular fiber cross-sectional shape, random asperity shape and RMS asperity height=0.8 μm but with different fiber diameters.

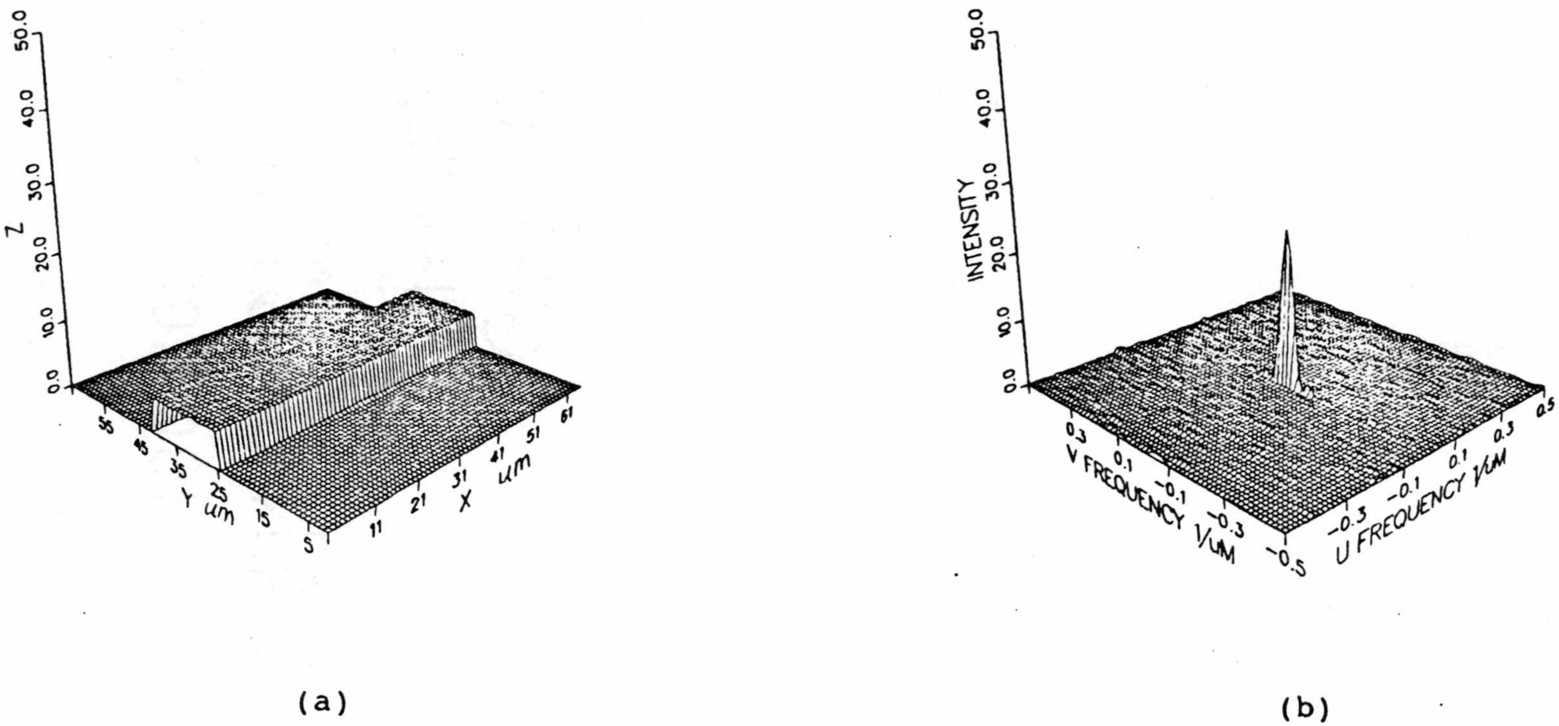

Figure 3.18: a) Fiber model with rectangular fiber cross-sectional shape, random asperity shape and RMS asperity height=0.08 μm, b) Fourier transform (theoretical scattering pattern) of the fiber model and computed RC=8.68.

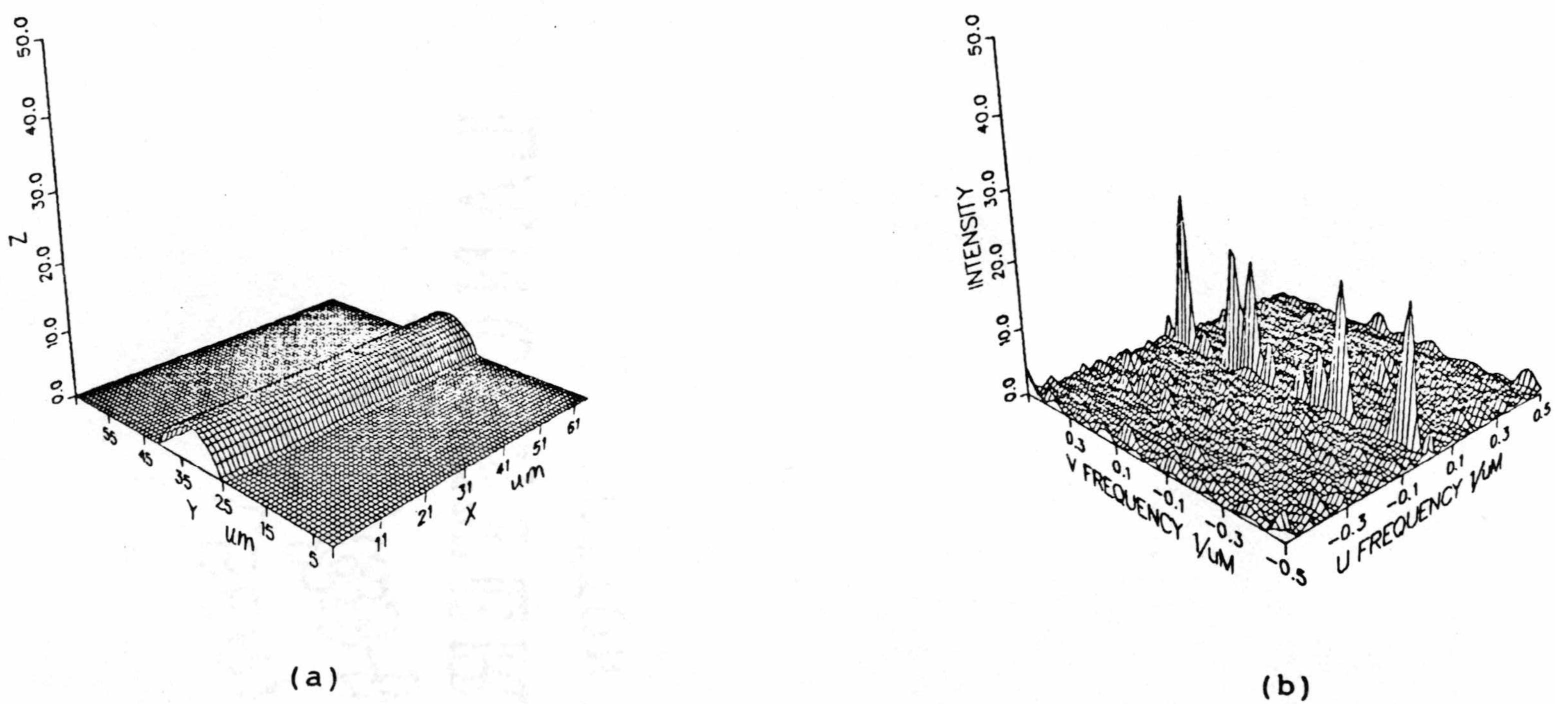

Figure 3.19: a) Fiber model with circular fiber cross- sectional shape, random asperity shape and RMS asperity height= 0.08 μm, b) Fourier transform (theoretical scattering pattern) of the fiber model and computed RC=8.68.

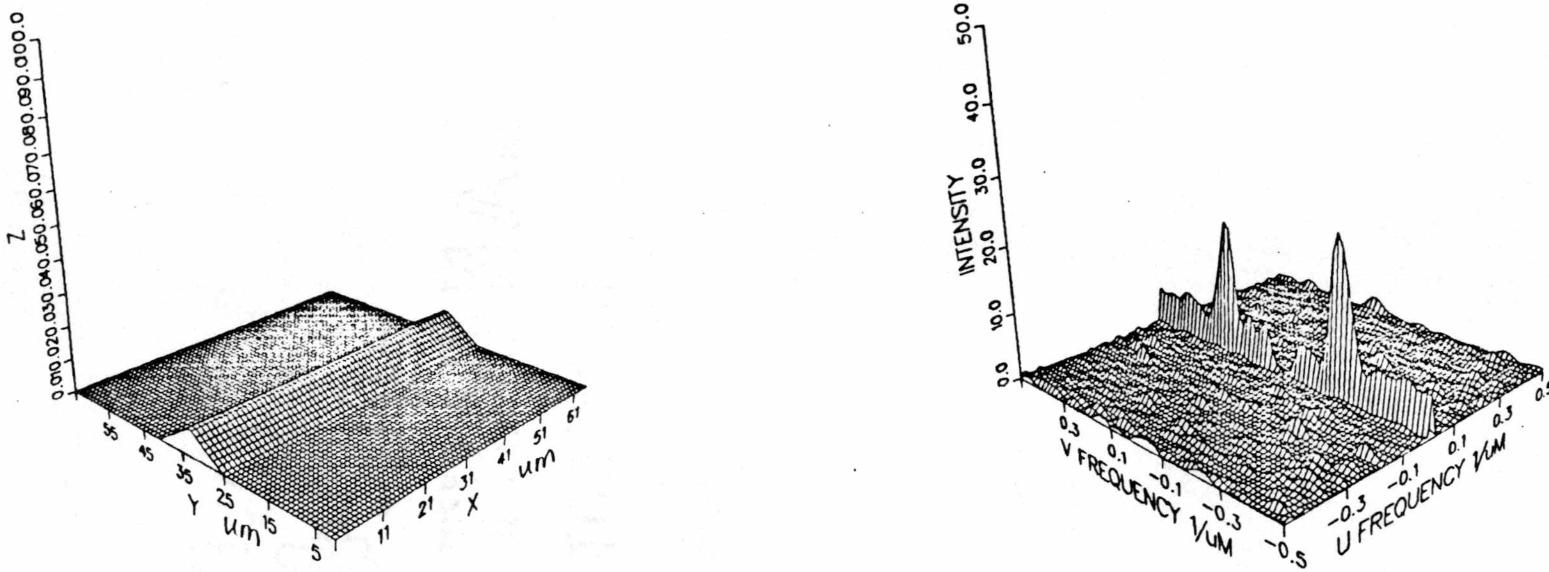

(a) (b)

Figure 3.20: a) Fiber model with triangular fiber cross- sectional shape, random asperity shape and RMS asperity height= 0.08 μm, b) Fourier transform (theoretical scattering pattern) of the fiber model and computed RC=5.34.

CHAPTER IV

OPTICAL SYSTEM DEVELOPMENT AND DISCUSSION

In the previous chapter, the theoretical dependence of scattering on fibers was examined. In this chapter scattering patterns from actual fibers are examined and relationships between actual scattering patterns and theoretical patterns are discussed. Two methods of detecting and analyzing scattering patterns are presented. The first method involves a vidicon-camera and micro-computer for two-dimensional analysis and the second method involves a simpler apparatus composed basically of two photo-detectors.

4.1 MICRO-COMPUTER BASED MEASURING SYSTEM

4.1.1 MEASURING SYSTEM APPARATUS

The micro-computer based measuring system developed at the SALS Lab, University of Tennessee[30] was modified for measurement of back scattering. The instrument used is shown schematically in figure 4.1. All optical components are mounted on a graduated 2 meter optical rail. The light source is a 2mw He-Ne laser. The sample holder permits 360^o rotation about the beam direction, as well as translation in the vertical and transverse directions. The scattered radiation is projected onto a Mylar imaging screen. The mylar screen is optically translucent, and thus allows the scattered image to be viewed from the rear of the screen by

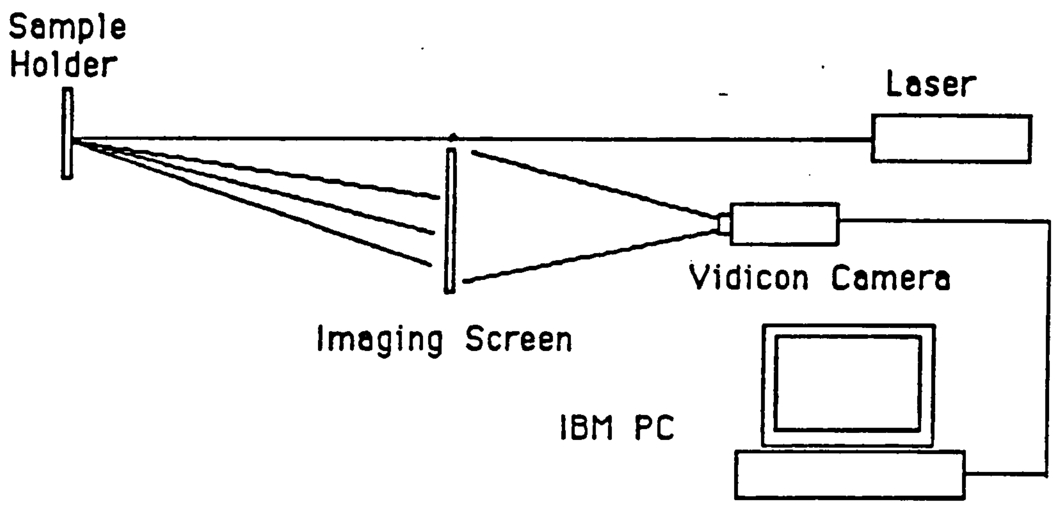

Figure 4.1: Micro-computer based measuring system.

the camera. An silicon-vidicon camera is used to detect the projected image. The signal output from the video camera is connected to an IBM personal computer equipped with a video digitizer interface card, 640 KB of user ram memory, two 360 KB floppy disk drives, an external 20 MB hard disk drive, a pen plotter, and a dot matrix printer. The digitized scattering patterns are stored on the 20 MB hard disk.

Fiber specimens are mounted on the rotatable sample holder and illuminated by the laser. The distance between sample and image screen should meet the restriction of Eq. (2.14) to satisfy the Fraunhofer diffraction requirement. After adjusting the camera for the optimum image, the back scattering pattern was digitized using the Video Van Gogh software package and saved on the hard disk for data analysis. If desired, the scattering pattern (spectrum) can be plotted by a pen plotter. A three-dimensional plot can also be obtained by using Goden software's SURF plotting packages. RC values were calculated by a user written routine.

Alternatively, the mylar imaging screen is replaced with a film holder and the back scattering pattern can be recorded on type 55 polaroid film.

4.1.2 RESULTS AND DISCUSSION

From the discussion in Chapter II, we know that light reflected from a perfectly smooth surface is found in the specular reflection. The intensity of this reflection depends upon the energy of the incident light, the angle of incidence and the optical properties of the sample. On the other hand, rough surfaces scatter light away from the specular direction and reduce it's intensity. This is illustrated in Figures 4.2 and 4.3 where the scattering patterns from fibers with four different levels of roughness were recorded by polaroid films.

Figure 4.2 (a) shows the back scattering pattern of a nylon fiber. Scattering from this fiber is predominantly specular, being intense and quite narrow. This indicates the fiber surface is very smooth. Figure 4.2 (b) shows the back scattering pattern of a polypropylene fiber. There are a little more scattered intensity than nylon. Figure 4.3 (a) shows the scattering pattern of a rayon fiber. The scattering is more diffuse than nylon and indicates the fiber surface is rougher than nylon in Figure 4.2 (a) and polypropylene in (b). Figure 4.3 (b) shows the scattering pattern of a wool fiber. The specular reflection is greatly diminished by diffuse scattering. This means that the wool fiber is quite rough. Figures 4.4 and 4.5 are back scattering patterns from the same fibers recorded with the vidicom camera and plotted three-dimensionally. As described earlier, the zero frequency intensity reduced and high frequency intensities increased following fiber surface from smooth to rough. The calculated RC values from these plots are 0.90, 1.84, 4.20, and 12.70 respectively for nylon, polypropylene, rayon and wool. The RC values for those fibers are in accordance with the visual results of the scattering patterns.

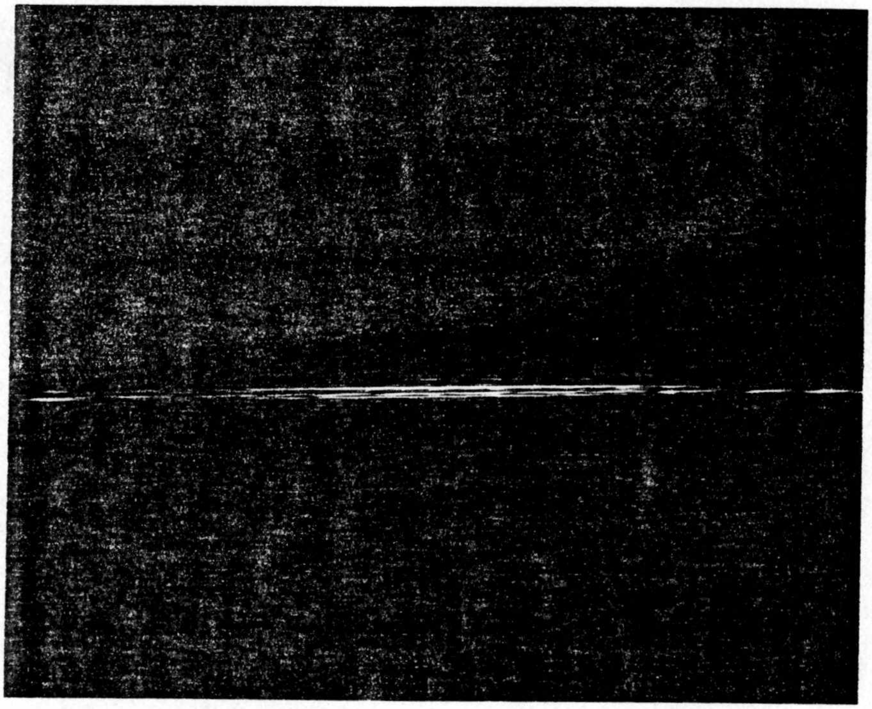

(a)

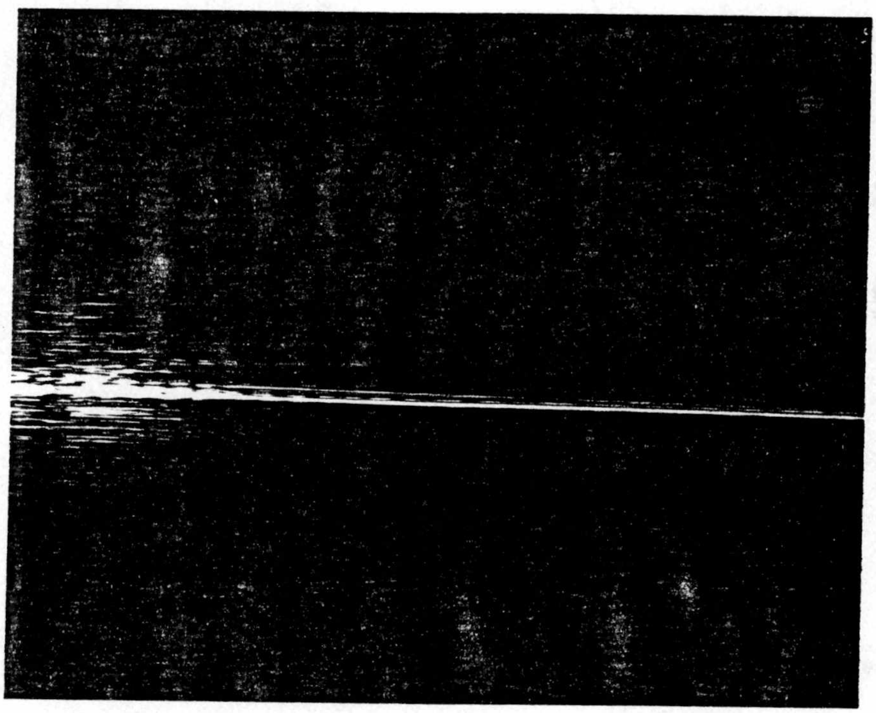

(b)

Figure 4.2: Back scattering patterns recorded on polaroid films, a) nylon and b) polypropylene fibers. The (0,0) point is located approximately 8 mm off the left center of each photograph.

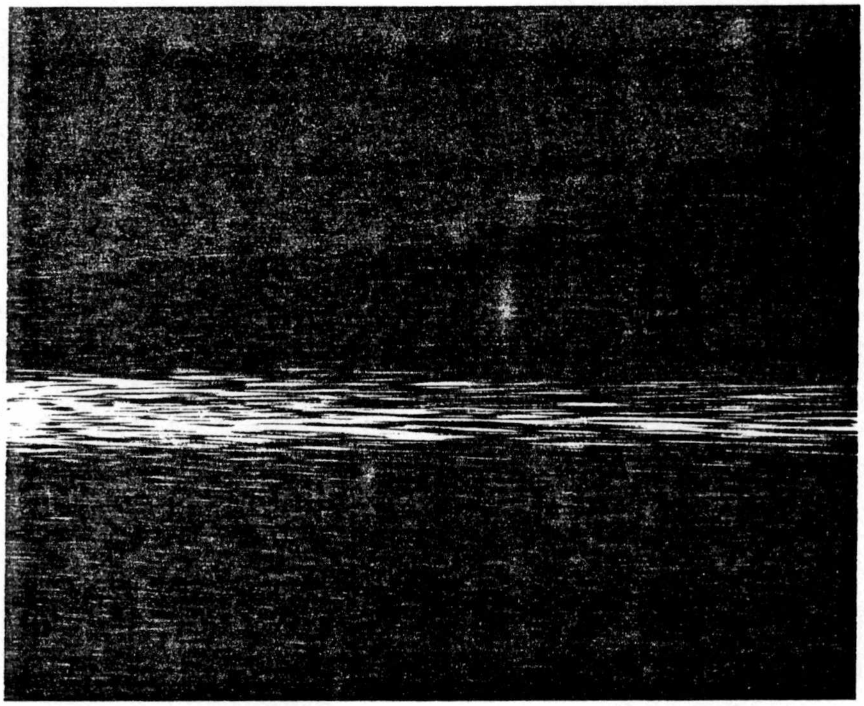

(a)

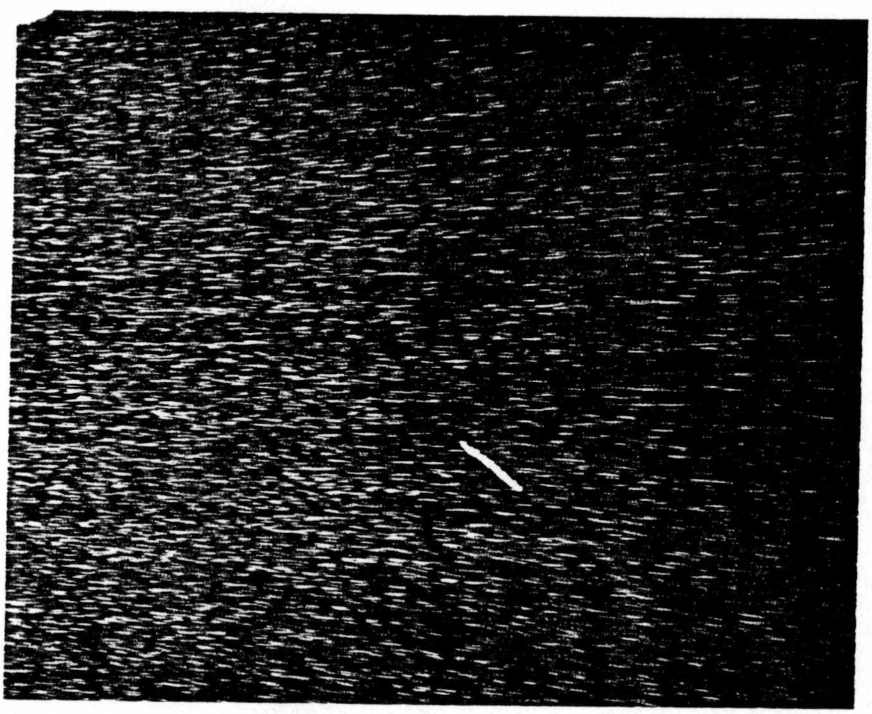

(b)

Figure 4.3: Back scattering patterns recorded on polaroid films, a) rayon and b) wool fibers. The (0,0) point is located approximately 8 mm off the left center of each photograph.

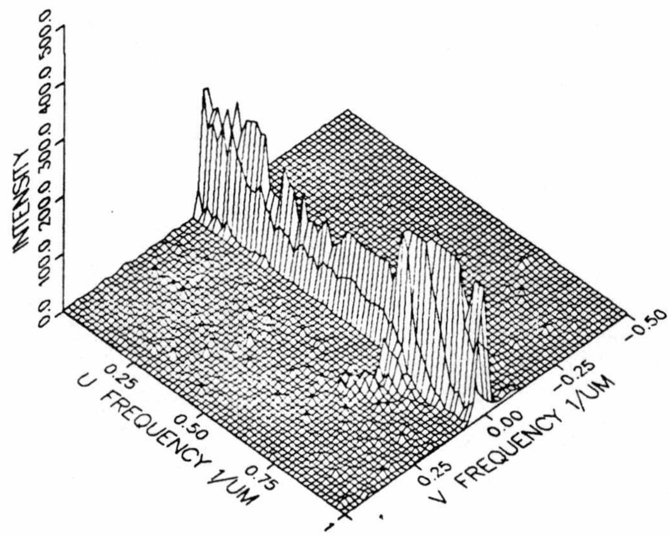

(a)

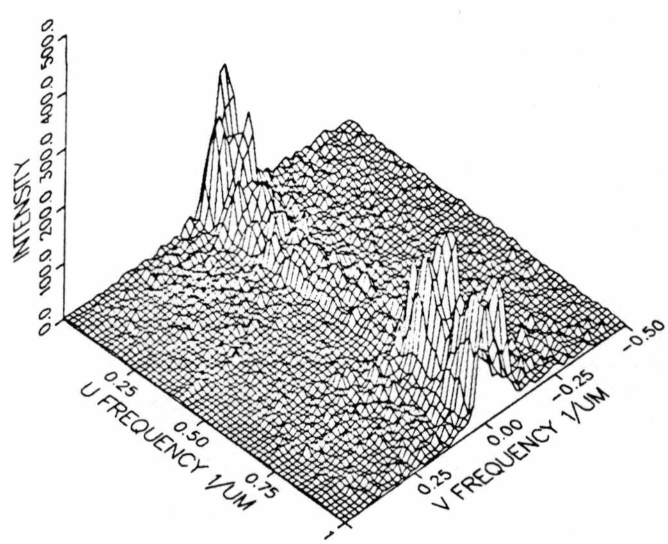

(b)

Figure 4.4: Three-dimensional plots of back scattering patterns from fibers: a) nylon, RC=0.90 and b) polypropylene, RC=1.84.

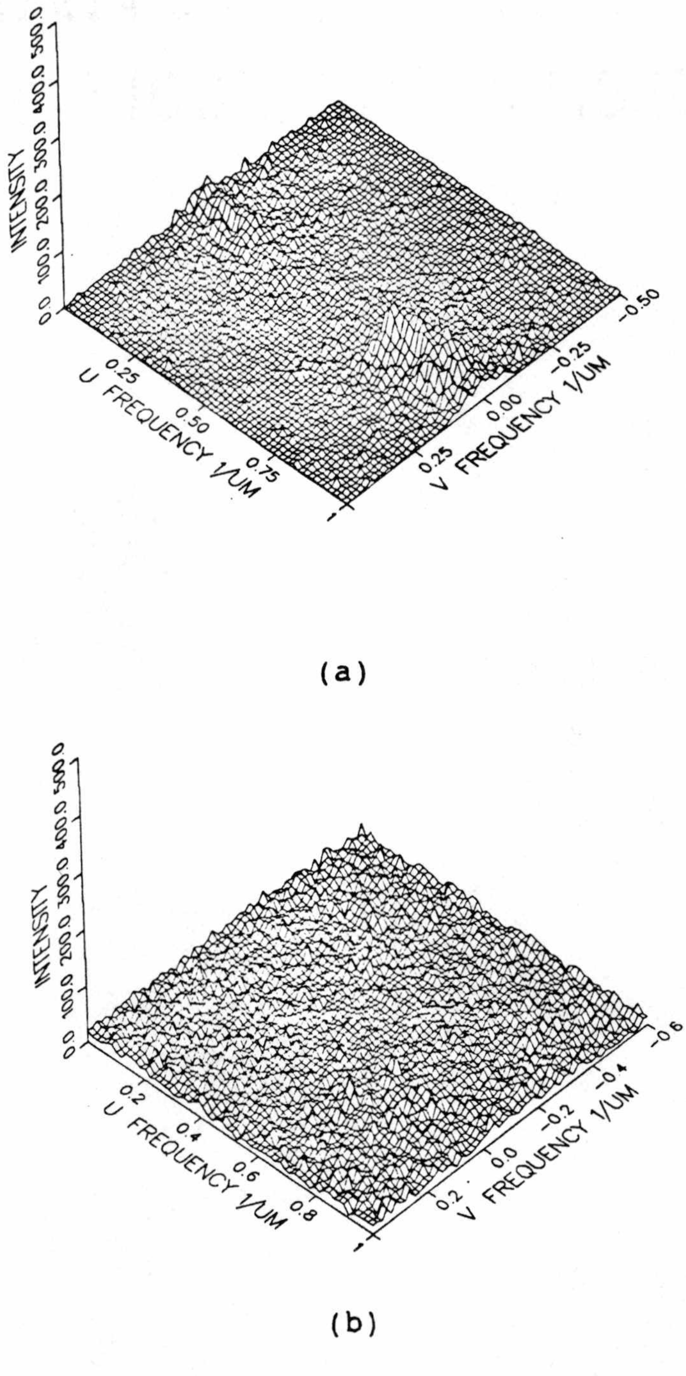

Figure 4.5: Three-dimensional plots of back scattering patterns from fibers a) rayon, RC=4.20 and b) wool, RC=12.70.

These experiments show that the vidicon camera system effectively capture two-dimensional data and perform subsequent analysis, especially for spatial-frequency analysis. However, when we only require a relative measure of fiber surface roughness, we need only measure the ratio of zero frequency intensity and other frequency intensities. The equipment can be simplified to reduce cost. Simple equipment is discribed in the next section and applied to some practical problems.

4.2 SIMPLE INSTRUMENT FOR ROUGHNESS MEASUREMENT

4.2.1 DESCRIPTION OF THE INSTRUMENT

Practical considerations of a measuring system are that it should be designed as simple as possible and be as versatile as possible. An essential requirement to obtain scattering spectrum of a surface is that it satisfies the conditions of Fraunhofer (far-field) diffraction. By using a converging spherical lens, this distance can be reduced and a two-dimensional Fourier transformation of the scatterer can be found in the focal plane of the lens. Therefore, the focal plane of a Fourier transform lens is also called Fourier transform plane.

Figure 4.6 illustrates a simple measuring system for obtaining the optical Fourier transform of a scatter. A He- Ne laser with a wavelength equal to 0.6328 um serves as the light source. A shutter is positioned in front of the laser to provide various exposure times when a photograph of the scattering pattern is

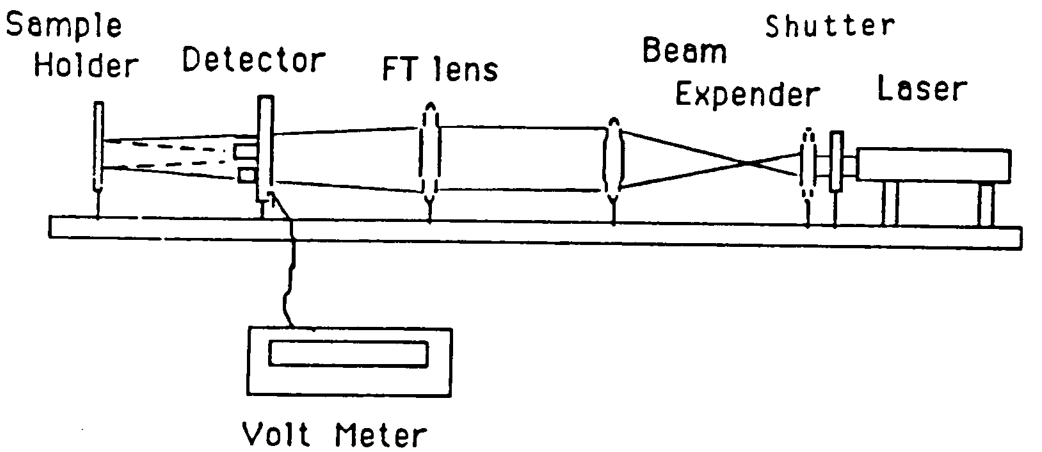

Figure 4.6: Simple optical Fourier transform system.

desired. Next is a Fourier transform lens of focal length = 400 mm. A photodetector device is mounted on a two-dimensional positioner, which is positioned in the Fourier transform plane, by locating it 120 mm from the sample holder and 280 mm from the FT lens. A polaroid film holder can be located in place of the photodector to photographically record back scattering patterns.

The photo-detector device is composed of two photo- transistors. The upper photo-transistor is positioned at zero frequency and is covered with a mask shaped to allow a narrow slit of zero frequency light to reach the detector but stop non-zero frequency components. The lower photo- transistor is used to collect non-zero frequency components. Signals from each detector are amplified by uA741 operational amplifiers and light intensities are measured in volts.

The general procedure for obtaining the roughness coefficient of a sample is as follows: First, the sample is placed on the sample holder and positioned in the center of the illuminating laser beam. Second, the location of the photo-transistor recording zero frequency scatter is adjusted until its voltage is maximized. The voltages from each photo-detector is recorded, one corresponding to the zero frequency component, I_o, and the other corresponding to the non-zero frequencies, I_t. The Roughness Coefficient is computed from these two readings using $R = I_t/I_0$.

A limitation of this measuring system is the detector. Using one phototransistor to collect diffuse scattered intensities provides only an approximate measure of light scattered from zero and non-zero spatial frequencies. This limitation is due to the response curve of the photo- transistor which is not linear. Another aspect of photodector that limits measurement accuracy is the region in space through which the detector gathers light. The photodector used to provide a measure of light scattered from nonzero frequencies gathered light from a region in space represented by about 15^{o} cone. A more accurate measure of diffuse scatter would be obtained if several photo- transistors were used or a linear CCD image sensor was used instead of one photo-transistor.

4.2.2 RESULTS AND DISCUSSION

ROUGHNESS EVALUATION

Two sample sets were used to investigate the use of roughness coefficient measured with the simple instrument employing two photodetors for roughness characterization. One set consisted of several types of fibers that vary in surface roughness. These are nylon, polypropylene, rayon, cotton and wool, with nylon being the smoothest fiber and wool roughest. The other fiber set consists of rayon fibers, which vary in luster.

Table 1 contains roughness coefficient values for one sample set. Nylon can be seen to have the smallest roughness coefficient. This indicates that nylon has the smoothest surface of the four fibers examined. On the other hand, wool has the largest roughness coefficient. This results from the scales covering the fiber surface.

Table 1. Roughness Coefficient Values for Different Dibers.

	Nylon	Polypropylene	Rayon	Cotton	Wool
RC	0.019	0.362	1.550	5.350	7.415

Other fibers in this sample set have roughness coefficient values between that of nylon and wool. These results show that the optical transform method is able to discriminate between fibers of different surface and roughness coefficient values provide a simple measure of surface roughness. Comparing these results with those from the vidicon-camera based system, the relative order of fiber roughness is the same for both methods, although the absolute values of roughness coefficients are not the same. This can be expected since different regions of scatter are used for determining I_o and I_t by each method.

Four types of rayon comprised the second fiber set and measurements from thirty different specimens of each type are summerized in Table 2. Mean roughness coefficient values were measured to be 1.827 and 2.385 for the bright rayons (#2556 and #2581) and 3.342 and 3.420 for the extradull rayons (#4315 and #4316). Microscopic measurements showed that the variability among these fiber specimens was quite large and the large coefficient of variations for roughness coefficients reflects this variability.

Student's "t" tests were used to test for significant differences among the means and these results are presented in Table 3 for an alpha value of 0.05. A critical t-value of 2.00 must be exceeded for any two means to be significantly different. The two bright rayons were not found to be significantly different from each other. Although the t-test concluded that one of the bright rayons (#2556) was

Table 2. Roughness Coefficient Values for Rayon Fibers.

	Bright Rayon #2556	Bright Rayon #2581	Extradull Rayon #4315	Extradull Rayon #4316
Average RC	2.522	2.877	3.899	3.599
Standard Dev.	1.050	1.670	1.469	1.490
CV %	41.6 %	58.1 %	37.6 %	41.4 %

Table 3. "t" Test for Sample set #2.

	Bright Rayon #2556	Bright Rayon #2581	Extradull Rayon #4315	Extradull Rayon #4316
#2556		0.130	4.106	3.182
#2581	0.130		2.474	1.737
#4315	4.106	2.474		0.772
#4316	3.182	1.737	0.772	

α=0.05 and critical t value=2.00

significantly different from the two extradull rayons, one bright rayon (#2581) and one extradull rayon (#4316) were concluded to be not different. The latter conclusion probably is affected by the large variation among fibers and might be reversed if more fiber samples were analyzed.

MEASURING THE EFFECT OF DELUSTERING

As discussed in chapter II, luster involves the appearance of a surface which exhibits specular reflections and delustering treatments which reduce specular reflections. Most delustering treatments involve deposition of particles in fibers which scatter light which falls on the fiber surface. The reduction of specular reflection and increase in diffuse scatter lead to a reduction in fiber luster. One application of the instrument used in this study might be the measurement of delustering effects on single fibers.

A fiber sample set was prepared by mixing T_iO_2 particles in melted polyethylene in concentrations of 0, 0.5 1, 2, and 5% Fibers with diameters of 40,120,and 160 um were hand pulled from the melt. Results of scattering are summarized in Table 4 and plotted in Figure 4.7. These results show that fiber surface roughness increased quickly with small additions of T_iO_2 and then increase farther with greater T_iO_2 concentrations.

Figures 4.8 and 4.9 show representative scattering patterns from each of the T_iO_2 concentrations. These patterns show qualitatively that increasing concentra-

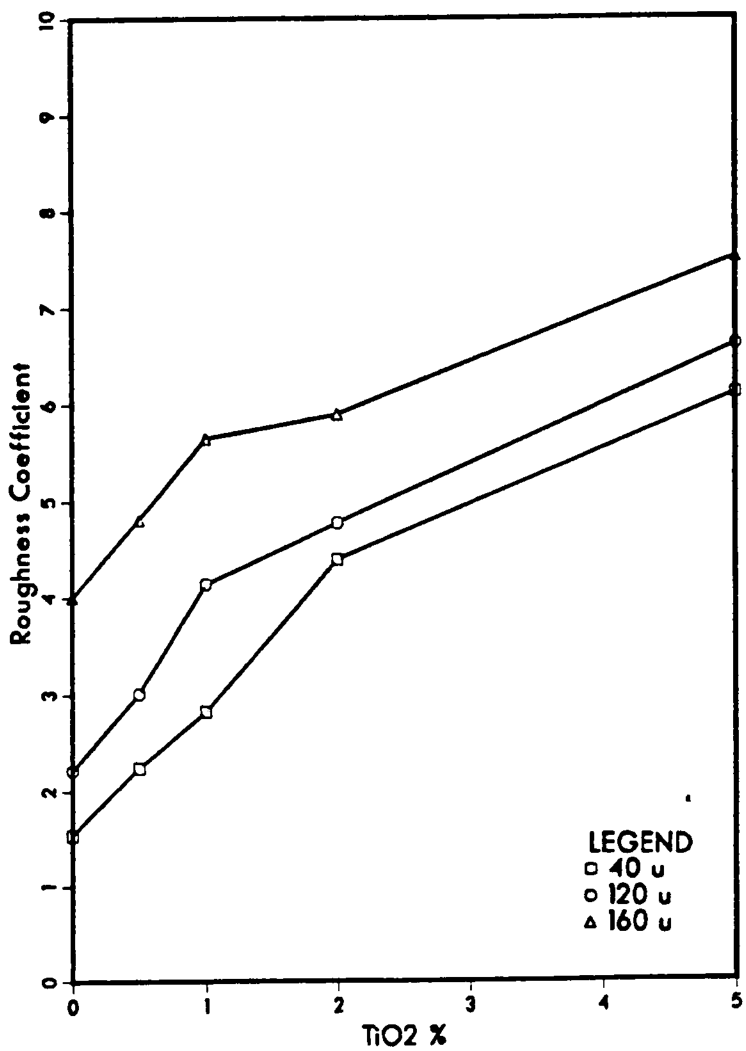

Figure 4.7: The delustering effect from $T_iO_2^*$. * each RC value is the mean of 10 specimens.

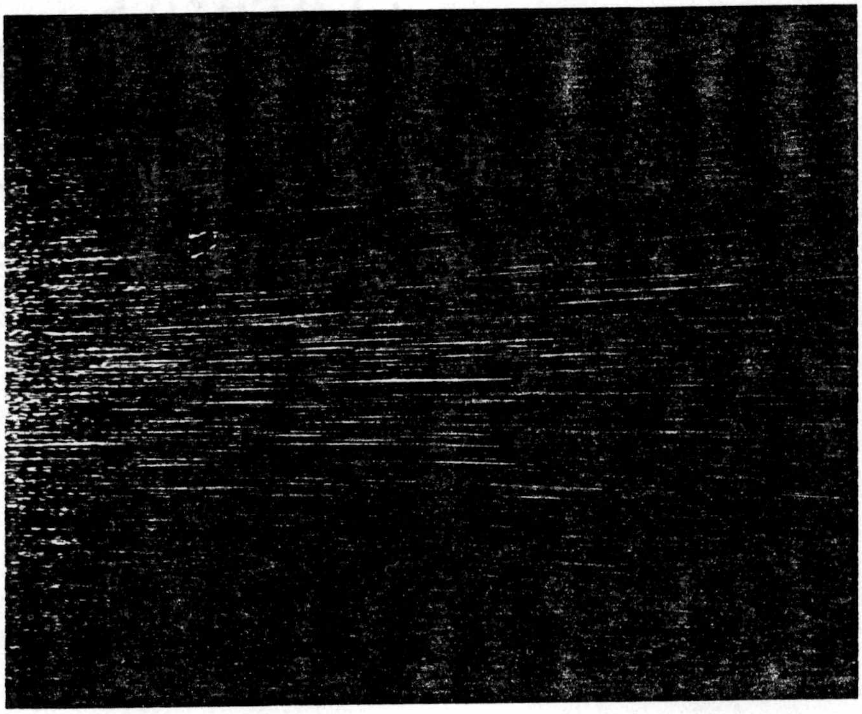

(a)

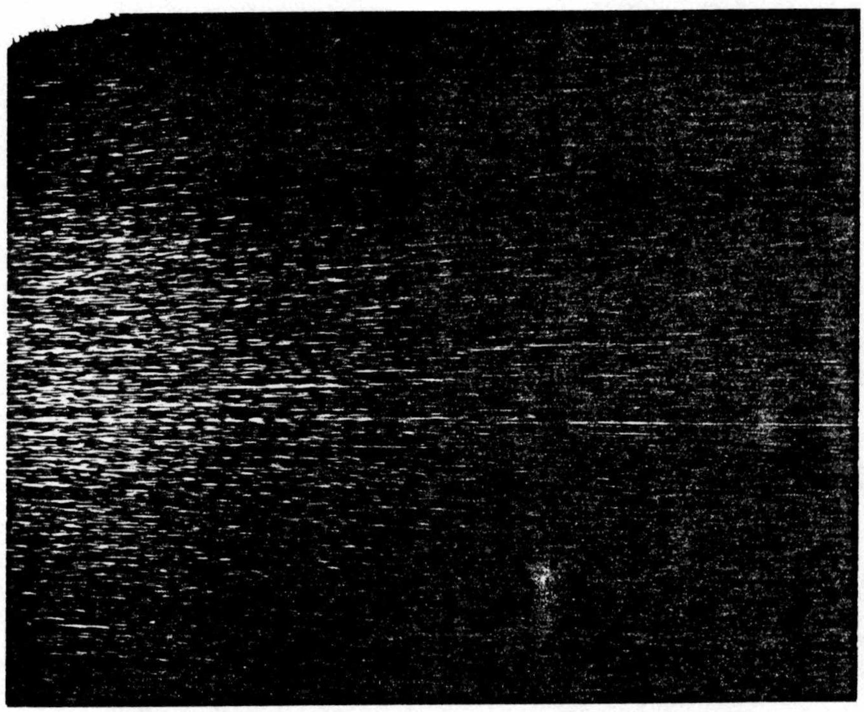

(b)

Figure 4.8: Back scattering patterns of $40\mu m$ diameter polyethylene fibers with T_iO_2 concentrations of a) 0.5% and b) 1.0%.

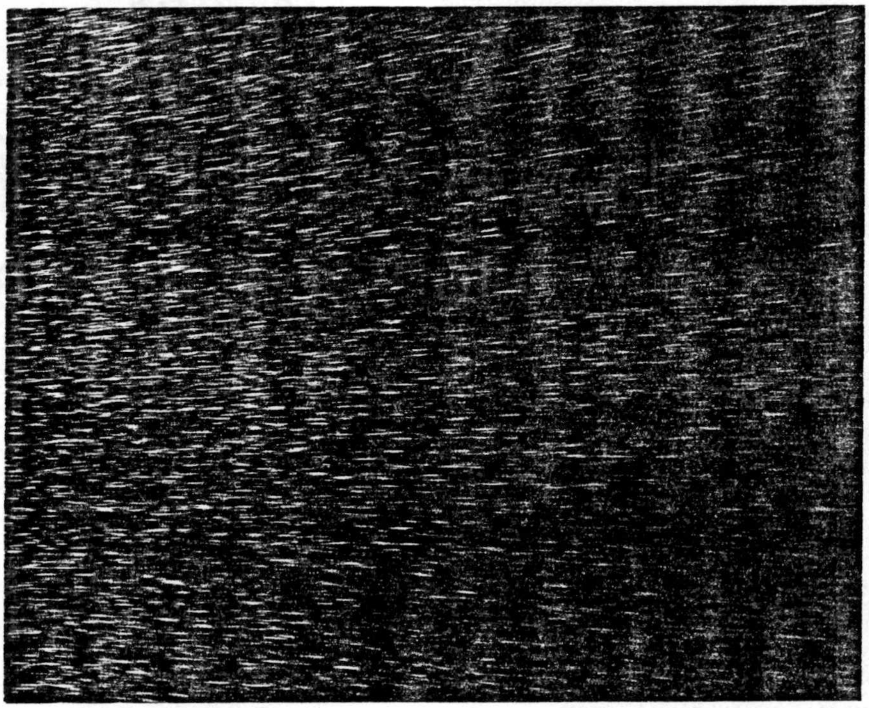

(a)

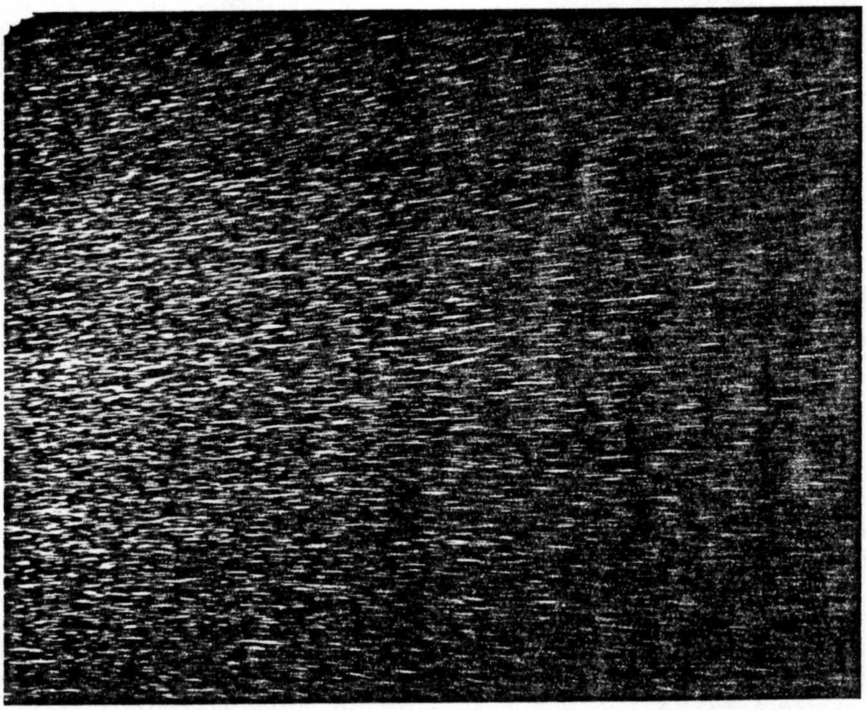

(b)

Figure 4.9: Back scattering patterns of $40\mu m$ diameter polyethylene fibers with T_iO_2 concentrations of a) 2.0% and b) 5.0%.

Table 4. RC Values for Delustered Polyethylene Fibers.

Fiber Diameter	T_iO_2 %				
	0 %	0.5 %	1 %	2 %	5 %
40 u	1.548	2.241	2.822	4.386	6.110
120 u	2.212	3.005	4.134	4.768	6.609
160 u	4.003	4.805	5.896	5.649	7.510

* each RC value is the mean of 10 speciems

tions of T_iO_2 result in increasing intensities of high frequency scattering components so fiber surface waviness shifts towards higher frequencies with increasing amounts of T_iO_2 deposition.

This method of luster measurement involves measurement of scattering from single fibers rather than yarns or fabrics as has been done in previous studies. Evaluation of luster should logically first involve measurements from single fibers and yarns or fabrics late. In this way, the contributions of fiber, yarn and fabric structure to luster may be separated.

MEASUREMENT OF CRYSTALLIZATION RATE

Crystallization in polymers is not only of theoretical interest for understanding polymer morphology but also of practical importance in many processing activities such as melt extrusion. Polymers that have been bulk crystallized under quiescent conditions contain polycrystalline structures called spherulites. These roughly spherical structures can be detected by either polarized optical microscopy or small-angle light scattering in the forward direction. In this study, we investigated the use of light back scattering as another method of detecting crystallization. In contrast of polarized optical microscopy and forward small-angle light scattering which provide information about bulk crystallization, the back scattering technique provides information about surface crystallization. Measurements of surface crystallization would be particularly beneficial for understanding some processes such as melt blowing which involve rapid surface cooling and consequent surface crystallization during processing.

Crystallization was examined in this study by melting polyethylene, and hand drawing fibers from the melt. A fiber then was heated above its melting point on a glass plate, quickly mounted on the instrument sample holder and allowed to cool at room temperature. Surface scattering was measured from the molten state through crystallization to the solidified state. Results are shown in Figure 4.10. The data clearly shows an abrupt increase in surface roughness and relatively constant RC values on both side of the rapid change. The abrupt change in the curve results from crystallization as verified by microscope that causes an increase in fiber surface roughness. Figure 4.11 shows scattering patterns before and after crystallization. The increase in diffuse scatter that accompanies crystallization is clearly evident in these photographs. This simple experiment shows that roughness measurements can be used to detect surface crystallization.

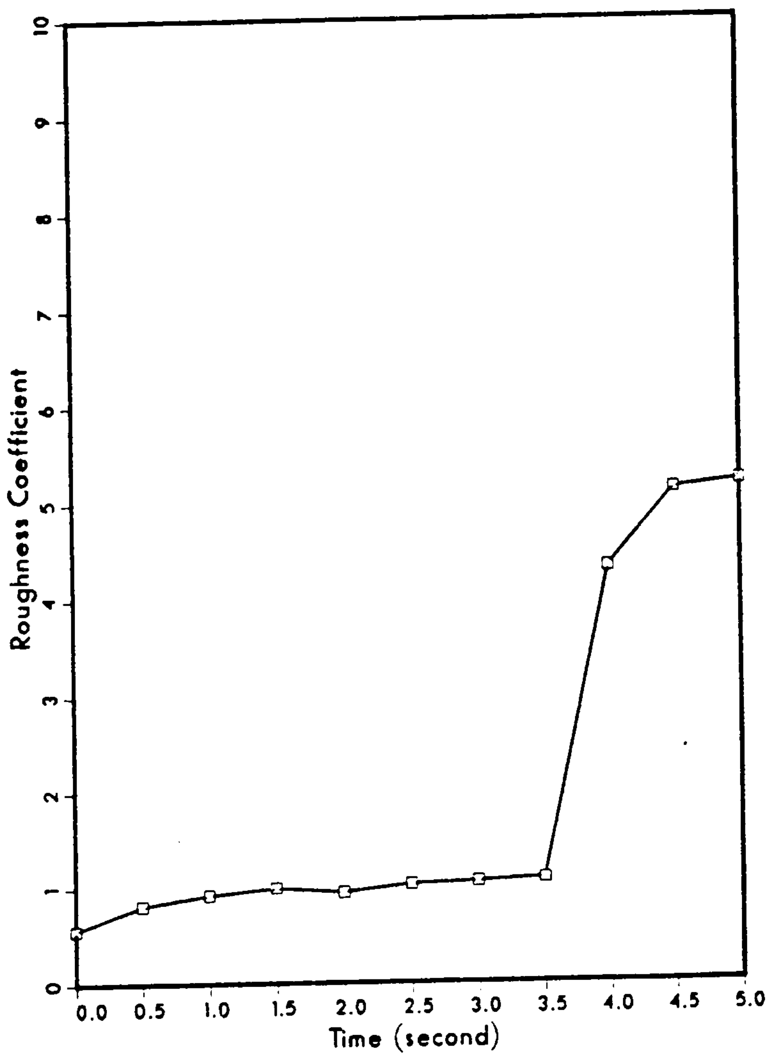

Figure 4.10: Roughness coefficient of polyethylene during crystallization.

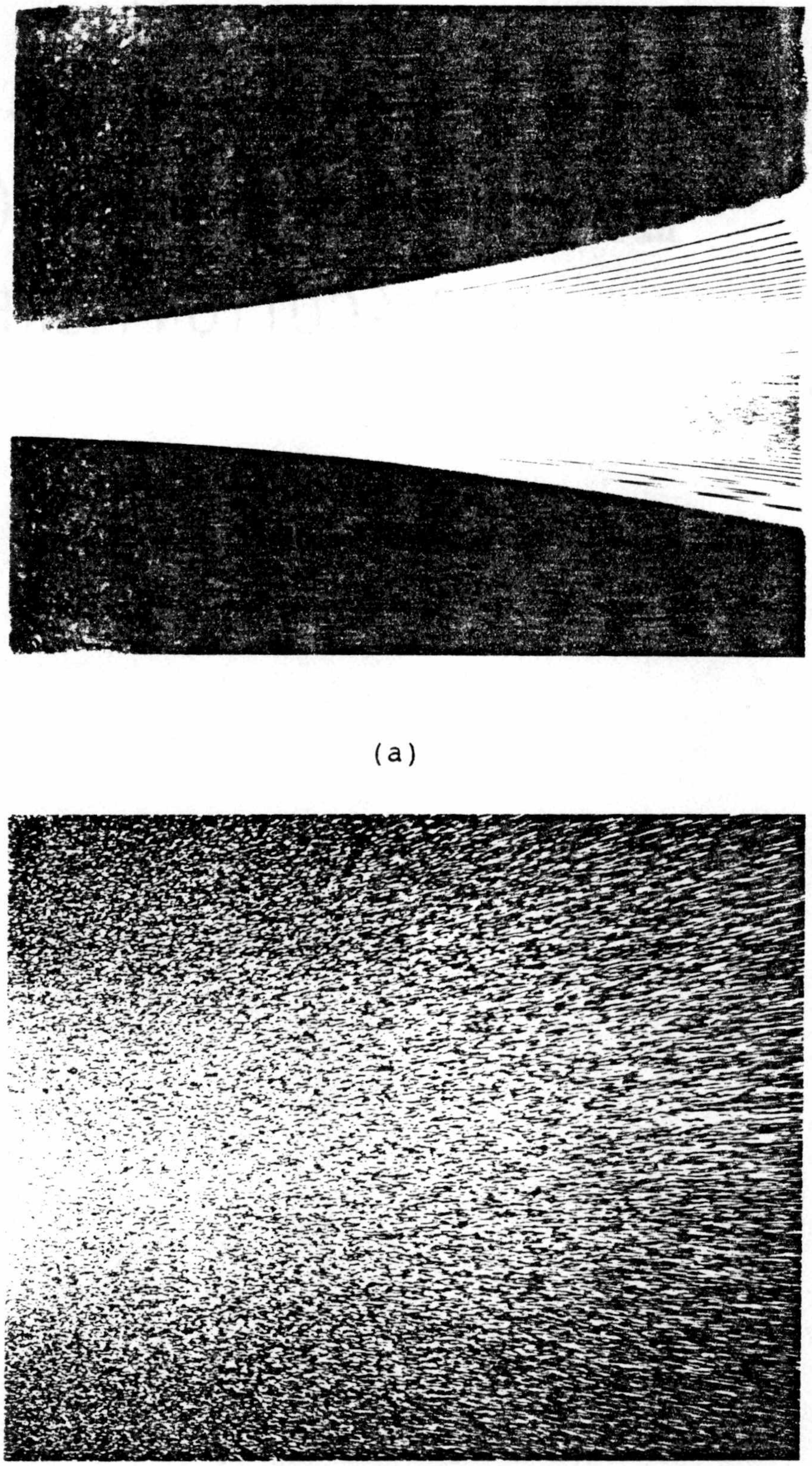

(a)

(b)

Figure 4.11: Back scattering patterns of polyethylene fibers, a) before and b) after crystallization.

CHAPTER V

SUMMARY AND CONCLUSIONS

Typical textile fibers have large surface-to-volume ratios, so their surface structure greatly influences many properties of fibrous materials. In addition, the surface structure of individual fibers often significantly affects their processing behavior during manufacture of other textile materials. Prominent among surface structure is geometric roughness. The application of laser back scattering to fiber surface roughness characterization was studied from both theoretical and experimental approaches. This study reveals relationships between back scattering patterns and fiber surface roughness. The hypothesis that the back scattering pattern is the Fourier transform of the reflectance from the fiber surface was verified. Good qualitative agreement between theoretically computed scattering patterns and actual measured back scattering patterns were obtained. A computer simulation study was employed to investigate the influence of fiber cross- sectional shapes and surface asperity shapes on back scattering patterns. Results show that the changes in cross- sectional shape will affect the intensity distribution in the direction perpendicular to the fiber axis, whereas the changes in asperity shape will affect the intensity distribution in the direction of paralled to the fiber axis.

In order to quantify roughness, a parameter "Roughness Coefficient" was defined as the ratio of scattered intensities and specular intensities at the zero-frequency. Applications of this parameter proved to be quite usefull. Two instruments were used to measure fiber surface roughness based on laser back scattering. One involved a vidicon- camera and micro-computer and the other instrument involved only two photo-detectors. Several applications have been examined, such as measuring the effect of "delustering" fibers with T_iO_2 and detecting crystallization. The results agree with practical experience. In conclusion, the optical transform method discussed in this thesis seems to have potential as a simple means of providing nonintrusive, real- time measurements of fiber surface structure during processing or after use in service.

RECOMMENDATIONS

As mentioned in the previous chapter, even minute changes in a fiber's surface structure may be measured with its back scattering pattern. Therefore, further applications need to be explored in the field of textile finishing and processing. It is also recommended that future studies might lead towards fiber identification. Combined with image processing and pattern recognition techniques, fibers with different surface structure might be classified automatically.

LIST OF REFERENCES

LIST OF REFERENCES

1. K. H. Guenther, P. G. Wierer, and J. M. Bennett. "Surface Roughness Measurements of Low-Scatter Mirrors and Roughness Standards." Applied Optics, Vol. 23, No. 21/1 Nov. 1984.

2. P. Beckmann, and A. Spizzichino. The Scattering of Electromagnetic Waves from Rough Surfaces. Pergamen Press, New York, 1963.

3. G. S. Buck, Jr and F. A. Mcload. "Luster and Cotton." Textile Research Journal Nov. 1949.

4. R. S. Hunter. "Methods of Determining Gloss." Nat. Bur. Standards (U.S.) J. Research 18, Jan. 1937, 19-39.

5. R. S. Hunter. "A multipurpose Photoelectric Reflectometer." Nat. Bur. Standards (U.S.) J. Research 25, Nov. 1940, 581-618.

6. R. Jeffries. "Measurement of the Extent of Delustering of Filament Fabrics." Journal of Textile Institute 47, 1956, T319.

7. L. Fourt et al. "The Improvement of Luster of Cotton. Part I: Measurement of Reflectance Characteristics Related to Luster." Textile Research Journal 21, July, 1951, 469-478.

8. F. L. Scardino and W. J. Lyons. "Fiber Surface Properties in Relation to Linear Assemblies During Processing. Part I." Textile Research Journal Oct. 1967.

9. D. Nickerson "A New Cotton Lustermeter for Yarns and Fibers." Textile Research Journal Feb. 1957, 111-123.

10. L. E. Holboke and L. P. Berriman. "A Study of the Effect of Cotton Fiber Structure on Luster." Textile Research Journal Mar. 1963.

11. S. C. Sheier and W. J. Lyons. "Measurement of the Surface Properties of Fibers" Resingraphic Methods, ASTM Special Technical Publication, 348, 1964.

12. J. Stover and S. Serati. "Calculation of Surface Statistics from Light Scatter." Optical Engineering 23, 1984, 406.

13. H. Fujii, T. Asakura, and Y. Shindo. "Measurement of

Surface Roughness Properties by Using Image Speckle Contrast." Journal of Optical Society of American 66, 1976, 1217.

14. J. Ohtsubo and T. Asakura. "Measurement of Surface Roughness Properties Using Speckle Patterns With Non-Gaussion Statistics." Optical Communication 25, 1978, 315.

15. D. Leger, E. Mathien, and J. Perrin. "Optical Surface Roughness Determination Using Speckle Correlation Technique." Applied Optics 14, 1975, 872.

16. H. Pedersen. "Object Roughness Dependence of Partially Developed Speckle Patterns in Coherent Light." Optical Communication 16, 1976, 63.

17. J. Goodman. "Dependence of Image Speckle Contrast on Surface Roughness." Optical Communication 14, 1975, 324.

18. J. Ohtsubo and T. Asakura. "Statistical Properties of Speckle Intensity Variations in the Diffraction Field under Illumination of Coherent Light." Optical Communication 14, 1975, 30.

19. H. E. Bennett. "Scattering Characteristics of Optical Materials." Optical Engineering 17, 1978, 480.

20. J. A. Detrio. "Light Scattering Surface Roughness Characterization." Proc. Soc. Photo-Opt. Instrum. Eng. 276, 1981, 136.

21. B. J. Pernick. "Surface Roughness Measurements with an Optical Fourier Spectrum Analyzer." Applied Optics 18, 1979, 796.

22. K. J. Allardyce and N. George. "Diffraction Analysis of Rough Reflective Surfaces." Applied Optics 26, June, 1987, 12-15.

23. M. J. Roberts. EE4490-Fourier Optics Handout 1987.

24. J. W. Goodman. Introduction to Fourier Optics McGraw-Hill, 1968.

25. A. Paponlis. Probability, Random Variables, and Stochastic Processes. McGraw-Hill, 1965.

26. R. C. Gonzalez and P. Wintz. Digital Image Processing. Addison Wesley, 1987.

27. H. Stark. Applications of Optical Fourier Transforms. Academic Press, 1982.

28. H. Lipson. Optical Transforms. Academic Press, 1972.

29. D. T. Clark and W. J. Feast. Polymer Surfaces. John Wiley & Sons, 1978.

30. L. J. Effler, Jr. "Quantitative Small Angle Light Scattering of Liquid Crystalline Copolyester Films." M.S. thesis, U. Tenn. 1987.

APPENDIX

```
C     ---------------------------------------------------
C
C     MAIN PROGRAM: LASER LIGHT BACK SCATTERING
C
C       THIS PROGRAM COMPUTED THEORETICAL BACK SCATTERING
C       PATTERN BASED ON THE FIBER MODEL.
C
C     MAJOR VARIABLES:
C       FIBER1: FIBER MODEL WITH RECTANGULAR CROSS SECTION.
C       FIBER2: FIBER MODEL WITH CIRCULAR CROSS SECTION.
C       FIBER3: FIBER MODEL WITH TRIANGLAR CROSS SECTION.
C       SLOPE : 1=RANDOM,2=SQUARE,3=TRIANGULAR,4=SINE.
C       MG    : A CONSTANT USED TO ADJUST RMS VALUE.
C       IAUTO : CONTROL THE SCALLING, 1: AUTO ADJUST OFF.
C       ID0   : FIBER DIAMETER.
C       ISCL  : LINEAR SCALE IF ISCL=0 AND LOG SCALE IF ISCL=1.
C       NM    : NUMBER OF DATA.
C
C
C     WRITTEN BY :
C                    CHENG LUO
C       DEPT OF TEXTILES AND MERCHANDISING
C       THE UNIVERSITY OF TENNESSEE
C       KNOXVILLE, TN 37996-1900
C
C     ---------------------------------------------------
C
      COMMON A(256,256)
      COMPLEX A1(256,256)
      INTEGER SLOPE
      NM=256
      M=8
      IST=-1
      ISCL=1
      WRITE(6,*)'INPUT FIBER MODEL NUMBER (1=RECTANGULAR, 2=CIRCULAR
     13=TRIANGULAR)'
      READ(5,*)FB
      WRITE(6,*)'INPUT SURFACE TYPE (1=RANDOM,2=SQUARE,3=TRIANGULAR,
     14=SINE)'
      READ(5,*)SLOPE
      WRITE(6,*)'INPUT MG (1-100)'
      READ(5,*)MG
      AMG=FLOAT(MG)
      WRITE(6,*)'INPUT FIBER DIAMETER (1-20)'
      READ(5,*)ID0
      FR=ID0/2.0
      ID1=IFIX(128-FR)
      ID2=IFIX(128+FR)
      WRITE(6,*)'INPUT AUTO (0,1) (1=AUTO ADJUST OFF)'
      READ(5,*)IAUTO
      GOTO (1,2,3),FB
 1    CALL FIBER1(NM,ID1,ID2,AMG,SLOPE)
      GOTO 6
 2    CALL FIBER2(NM,FR,AMG,ID1,ID2,SLOPE)
      GOTO 6
 3    CALL FIBER3(NM,AMG,ID1,ID2,SLOPE)
 6    WRITE(21,600) ((I-95,J-95,A(I,J),I=96,160),J=96,160)
 600  FORMAT(1X,I4,1X,I4,1X,F8.2)
      WRITE(19,650) (I-95,A(I,129),I=96,160)
 650  FORMAT(1X,I4,2X,F6.2)
      CALL SDV(ID1,ID2,SD,NM)
      RMS=SD
      CALL CEV(ID1,ID2,CV,NM)
      CALL REFLCT(A1,NM,ID1,ID2,ISCL,IAUTO)
      CALL CENTER(A1,NM)
      CALL TFFT(A1,N,M,NM,ISCL,IAUTO)
```

```
      DO 10 I=1,256,2
        DO 20 J=1,256,2
          XA=(I-128)/256.0
          YA=(J-128)/256.0
          WRITE(20,700) XA,YA,A(I,J)
 700      FORMAT(1X,F6.3,1X,F6.3,1X,F8.2)
 20     CONTINUE
 10   CONTINUE
      DO 30 I=1,256
        XA=(I-128)/256.0
        WRITE(16,750) XA,A(I,129)
 750    FORMAT(1X,F6.3,2X,F6.2)
 30   CONTINUE
      CALL RC(R,NM)
      CALL SDV(1,256,SD,NM)
      WRITE(22,100)
 100  FORMAT(5X,6H RMS  ,4X,6H  CV  ,4X,6H  RC  ,4X,4H  SD)
      WRITE(22,200) RMS,CV,R,SD
 200  FORMAT(5X,F6.2,4X,F6.2,4X,F6.2,4X,F6.2,4X,F6.2)
      STOP
      END
C
C     ---------------------------------------------------
C
C     THIS SUBROUTINE CENTERS THE OUTPUT BY MULTIPLYING
C     (-1)**(X+Y) WITH F(X,Y).
C
C     ---------------------------------------------------
C
      SUBROUTINE CENTER(A1,NM)
      COMPLEX A1(256,256),A2
      A2=CMPLX(-1.0,0.0)
      DO 10 I=1,NM
        DO 20 J=1,NM
          A1(I,J)=A1(I,J)*A2**(I+J)
 20     CONTINUE
 10   CONTINUE
      RETURN
      END
C
C     -----------------------------------------------------------------
C
C       THIS SUBROUTINE PERFORMS TWO-DIMENSIONAL FOURIER TRANSFORM ON
C       THE FIBER MODEL BASED ON THE METHOD DESCRIBED IN THE BOOK
C       "DIGITAL IMAGE PROCESSING" BY R.C.GONZALEZ AND P.WINTZ.
C
C     -----------------------------------------------------------------
C
      SUBROUTINE TFFT(A1,N,M,NM,ISCL,IAUTO)
      COMPLEX A1(256,256),A2(256)
      COMMON A(256,256)
      DIMENSION B(256,256)
C
C       Perform row transform.
C
      DO 30 I=1,NM
        DO 40 J=1,NM
          A2(J)=A1(I,J)
 40     CONTINUE
        CALL FFT(A2,M)
        DO 50 J=1,NM
          A1(I,J)=A2(J)*N
 50     CONTINUE
 30   CONTINUE
C
C       Perform column transform.
```

```
C
      DO 60 J=1,NM
        DO 70 I=1,NM
          A2(I)=A1(I,J)
 70     CONTINUE
        CALL FFT(A2,M)
        DO 80 I=1,NM
          A1(I,J)=A2(I)
 80     CONTINUE
 60   CONTINUE
C
C       Calculate power spectrum.
C
      DO 100 I=1,NM
        DO 110 J=1,NM
          B(I,J)=S(A1(I,J))
          B(I,J)=B(I,J)*B(I,J)
 110    CONTINUE
 100  CONTINUE
C
C       Scale the spectrum.
C
      CALL SCL(B,ISCL,NM,IAUTO)
      RETURN
      END
C
C     ------------------------------------------------------------------
C
C       THIS SUBROUTINE PERFORMS THE FFT CALLED BY SUBROUTINE "TFFT".
C
C     ------------------------------------------------------------------
C
      SUBROUTINE FFT(F,LN)
      COMPLEX F(1024),U,W,T,CMPLX
      PI=3.141593
      N=2**LN
      NV2=N/2
      NM1=N-1
      J=1
      DO 3 I=1,NM1
         IF (I.GE.J) GO TO 1
         T=F(J)
         F(J)=F(I)
         F(I)=T
 1       K=NV2
 2       IF (K.GE.J) GO TO 3
         J=J-K
         K=K/2
         GO TO 2
 3       J=J+K
      DO 5 L=1,LN
         LE=2**L
         LE1=LE/2
         U=(1.0,0.0)
         W=CMPLX(COS(PI/LE1),-SIN(PI/LE1))
         DO 5 J=1,LE1
            DO 4 I=J,N,LE
               IP=I+LE1
               T=F(IP)*U
               F(IP)=F(I)-T
 4             F(I)=F(I)+T
 5          U=U*W
      DO 6 I=1,N
 6       F(I)=F(I)/FLOAT(N)
      RETURN
      END
```

```
C
C     ------------------------------------------------------------------
C
C       THIS FUNCTION CALCULATES THE MAGNITUDE OF THE COMPLEX.
C
C     ------------------------------------------------------------------
C
      FUNCTION S(C)
      COMPLEX C
      R=REAL(C)
      AI=AIMAG(C)
      S=SQRT(R**2+AI**2)
      RETURN
      END
C
C     ------------------------------------------------------------------
C
C       THIS SUBROUTINE SCALES THE MAGNITUDE FROM 0,...,TO 50 GRAY LEVEL.
C       IF PARAMETER ISCL=1, IT IS A LINEAR SCALE. IF ISCL=0, LOG SCALE.
C
C     ------------------------------------------------------------------
C
      SUBROUTINE SCL(B,ISCL,NM,IAUTO)
      COMMON A(256,256)
      INTEGER ISCL
      DIMENSION B(256,256)
      REAL CONST,S
C
C       Find the max value.
C
      AMAX=B(1,1)
      DO 10 I=1,NM
        DO 20 J=1,NM
          S=B(I,J)
          IF (S.GT.AMAX) THEN
            AMAX=S
          ENDIF
 20     CONTINUE
 10   CONTINUE
C
C       Perform linear scaling.
C
      IF (ISCL.EQ.1) THEN
        CONST=AMAX/48.0
        IF (IAUTO.EQ.1) CONST=1.0
        DO 30 I=1,NM
          DO 40 J=1,NM
            S=B(I,J)
            A(I,J)=S/CONST
 40       CONTINUE
 30     CONTINUE
      ELSE
C
C       Perform log scaling.
C
        CONST1=AMAX
        CONST=ALOG(CONST1+1.0)/48.0
        IF (IAUTO.EQ.1) CONST=1.0
        DO 50 I=1,NM
          DO 60 J=1,NM
            S1=B(I,J)
            S=ALOG(S1+1.0)/CONST
            A(I,J)=S
 60       CONTINUE
 50     CONTINUE
      ENDIF
```

```
      RETURN
      END
C
C     ---------------------------------------------------------------
C
C       THIS SUBROUTINE CALCULATES THE REFLECTANCE OF THE FIBER SERFACE.
C
C     ---------------------------------------------------------------
C
      SUBROUTINE REFLCT(R,NM,ID1,ID2,ISCL,IAUTO)
      COMMON A(256,256)
      DIMENSION B(256,256)
      COMPLEX R(256,256)
      DO 10 I=1,NM
        DO 20 J=1,NM
          R(I,J)=CMPLX(0.0,0.0)
 20     CONTINUE
 10   CONTINUE
      PI=3.1415926
      AK=4*PI/0.6328
      DO 30 I=1,NM
        DO 40 J=ID1,ID2
          HK=AK*A(I,J)
          R(I,J)=CMPLX(COS(HK),SIN(HK))
 40     CONTINUE
 30   CONTINUE
C
C       Calculate magnitude of the reflectance.
C
      DO 50 I=1,NM
        DO 60 J=1,NM
          B(I,J)=S(R(I,J))
 60     CONTINUE
 50   CONTINUE
      CALL SCL(B,ISCL,NM,IAUTO)
      RETURN
      END
C
C     ---------------------------------------------------------------
C
C       THIS SUBROUTINE GENERATES FIBER MODEL WHICH HAS RECTANGULAR
C       CROSS SECTION.
C
C     ---------------------------------------------------------------
C
      SUBROUTINE FIBER1(NM,ID1,ID2,AMG,SLOPE)
      COMMON A(256,256)
      INTEGER SLOPE
      DO 10 I=1,NM
        DO 20 J=1,NM
          A(I,J)=0.0
 20     CONTINUE
 10   CONTINUE
      GOTO (1,2,3,4),SLOPE
 1    CALL FIBER(NM,ID1,ID2)
      GOTO 5
 2    CALL SQUARE(NM,ID1,ID2)
      GOTO 5
 3    CALL TRIANG(NM,ID1,ID2)
      GOTO 5
 4    CALL SINE(NM,ID1,ID2)
 5    DO 30 I=1,NM
        DO 40 J=ID1,ID2
          A(I,J)=5.0+A(I,J)/AMG
 40     CONTINUE
 30   CONTINUE
```

```
      RETURN
      END
C
C     ------------------------------------------------------------------
C
C       THIS SUBROUTINE GENERATES FIBER MODEL WHICH HAS CIRCULAR CROSS
C       SECTION.
C
C     ------------------------------------------------------------------
C
      SUBROUTINE FIBER2(NM,FR,AMG,ID1,ID2,SLOPE)
      COMMON A(256,256)
      INTEGER SLOPE
      DO 10 I=1,NM
        DO 20 J=1,NM
          A(I,J)=0.0
 20     CONTINUE
 10   CONTINUE
      GOTO (1,2,3,4),SLOPE
 1    CALL FIBER(NM,ID1,ID2)
      GOTO 5
 2    CALL SQUARE(NM,ID1,ID2)
      GOTO 5
 3    CALL TRIANG(NM,ID1,ID2)
      GOTO 5
 4    CALL SINE(NM,ID1,ID2)
 5    DO 30 I=1,NM
        DO 40 J=ID1,ID2
          X=J-128
          Z=SQRT(FR*FR-X*X)
          A(I,J)=A(I,J)/AMG+Z
 40     CONTINUE
 30   CONTINUE
      RETURN
      END
C
C     ------------------------------------------------------------------
C
C       THIS SUBROUTINE GENERATES A FIBER MODEL WHICH HAS TRIANGULAR CROSS
C       SECTION.
C
C     ------------------------------------------------------------------
C
      SUBROUTINE FIBER3(NM,AMG,ID1,ID2,SLOPE)
      COMMON A(256,256)
      INTEGER SLOPE
      B=128-ID1
      DO 30 I=1,NM
        DO 40 J=1,NM
          A(I,J)=0.0
 40     CONTINUE
 30   CONTINUE
      GOTO (1,2,3,4),SLOPE
 1    CALL FIBER(NM,ID1,ID2)
      GOTO 5
 2    CALL SQUARE(NM,ID1,ID2)
      GOTO 5
 3    CALL TRIANG(NM,ID1,ID2)
      GOTO 5
 4    CALL SINE(NM,ID1,ID2)
 5    DO 10 I=1,NM
        DO 20 J=ID1,128
          X=J-128
          Z=X+B
          A(I,J)=A(I,J)/AMG+Z
 20     CONTINUE
```

```
         DO 50 J=128,ID2
           X=J-128
           Z=-X+B
           A(I,J)=A(I,J)/AMG+Z
 50      CONTINUE
 10    CONTINUE
       RETURN
       END
C
C      ---------------------------------------------------------------
C
C        THIS SUBROUTINE GENERATES A FIBER SURFACE WHICH HAS A GAUSSIAN
C        DISTRIBUTED RANDOM ROUGHNESS.
C
C      ---------------------------------------------------------------
C
       SUBROUTINE FIBER(NM,ID1,ID2)
       COMMON A(256,256)
       L=9999
       DO 10 J=ID1,ID2
         S=0.0
         DO 20 I=1,NM
           CALL RANDOM(Y,L,6.0)
           A(I,J)=Y
           S=S+A(I,J)
           L=L-1
 20      CONTINUE
         AM=S/NM
         DO 30 K=0,12
           D=FLOAT(K)
           B=D-1.0
           C=0.0
           DO 40 I=1,NM
             IF (A(I,J).GT.D) GOTO 40
             IF (A(I,J).LT.B) GOTO 40
             C=C+1.0
 40        CONTINUE
 30      CONTINUE
 10    CONTINUE
       RETURN
       END
C
C      -------------------------------------------------------------
C
C        THIS SUBROUTINE GENERATES GAUSSIAN DISTRIBUTED RANDOM NUMBERS.
C
C      -------------------------------------------------------------
C
       SUBROUTINE RANDOM(Y,L,AVE)
       REAL Y
       S1=0.0
       DO 10 I=1,12
         R=RAN(L)
         S1=S1+R
 10    CONTINUE
       Y=AVE+3.0*(S1-6.0)
       RETURN
       END

C
C      ---------------------------------------------------------------
C
C        THIS SUBROUTINE GENERATES SQUARE SURFACE PROFILE.
C
C      ---------------------------------------------------------------
C
```

```
      SUBROUTINE SQUARE(NM,ID1,ID2)
      COMMON A(256,256)
      INTEGER END
      L=9999
      DO 30 J=ID1,ID2
        I=1
C
C       Generate the width of square wave.
C
 50     CALL RANDOM(X,L,15.0)
        L=L-1
        X=ABS(X)
        END=IFIX(X)
        IF (END.EQ.0) END=1
C
C       Generate the height of square wave.
C
        CALL RANDOM(Y,L,6.0)
        L=L-1
        Y=ABS(Y)
        DO 10 K=0,END
          A(I,J)=Y
          IF (I.EQ.NM) GOTO 30
          I=I+1
 10     CONTINUE
        GOTO 50
 30   CONTINUE
      RETURN
      END
C
C     ----------------------------------------------------------------
C
C       THIS SUBROUTINE GENERATES TRIANGULAR SURFACE PROFILE.
C
C     ----------------------------------------------------------------
C
      SUBROUTINE TRIANG(NM,ID1,ID2)
      COMMON A(256,256)
      INTEGER END
      L=9999
      DO 30 J=ID1,ID2
        I=1
C
C       Generate the width of triangular wave.
C
 50     CALL RANDOM(X,L,15.0)
        L=L-1
        X=ABS(X)/2.0
        MID=IFIX(X)
        END=IFIX(X*2.0)
        IF (END.EQ.0) END=1
C
C       Generate the height of triangular wave.
C
        CALL RANDOM(Y,L,6.0)
        L=L-1
        Y=ABS(Y)
C
C       Calculate the slope.
C
        C=Y/X
        K1=0
        DO 10 K=0,MID
          A(I,J)=C*K1
          IF (I.EQ.NM) GOTO 30
          I=I+1
```

```
          K1=K1+1
 10     CONTINUE
        DO 20 K=MID+1,END
          A(I,J)=-C*K1+Y*2.0
          IF (I.EQ.NM) GOTO 30
          I=I+1
          K1=K1+1
 20     CONTINUE
        GOTO 50
 30   CONTINUE
      RETURN
      END
C
C     -----------------------------------------------------------------
C
C       THIS SUBROUTINE GENERATES SINE FURFACE PROFILE.
C
C     -----------------------------------------------------------------
C
      SUBROUTINE SINE(NM,ID1,ID2)
      COMMON A(256,256)
      INTEGER END
      L=9999
      PI=3.1415926
      DO 30 J=ID1,ID2
        I=1
C
C       Generate the width of sine wave.
C
 50     CALL RANDOM(X,L,15.0)
        L=L-1
        X=ABS(X)
        END=IFIX(X)
        IF (END.EQ.0) END=1
C
C       Calculate the height of sine wave.
C
        CALL RANDOM(Y,L,6.0)
        L=L-1
        Y=ABS(Y)
        DO 10 K=0,END
          A(I,J)=Y*SIN(K*PI/END)
          IF (I.EQ.NM) GOTO 30
          I=I+1
 10     CONTINUE
        GOTO 50
 30   CONTINUE
      RETURN
      END
C
C     -----------------------------------------------------------------
C
C       THIS FUNCTION CALCULATES THE MEAN.
C
C     -----------------------------------------------------------------
C
      FUNCTION AMEAN(J,NM)
      COMMON A(256,256)
      S=0.0
      AN=FLOAT(NM)
      DO 10 I=1,NM
        S=A(I,J)+S
 10   CONTINUE
      AMEAN=S/AN
      RETURN
      END
```

```
C
C     ----------------------------------------------------------------
C
C       THIS SUBROUTINE CALCULATES CV% .
C
C     ----------------------------------------------------------------
C
      SUBROUTINE CEV(ID1,ID2,CV,NM)
      COMMON A(256,256)
      TMEAN=0.0
      DO 10 J=ID1,ID2
        TMEAN=TMEAN+AMEAN(J,NM)
10    CONTINUE
      TMEAN=TMEAN/(ID2-ID1)
      CALL SDV(ID1,ID2,SD,NM)
      CV=SD/TMEAN
      RETURN
      END
C
C     --------------------------------------------------------------------
C
C       THIS SUBROUTINE CALCULATES THE STANDARD DEVIATION.
C
C     --------------------------------------------------------------------
C
      SUBROUTINE SDV(ID1,ID2,SD,NM)
      COMMON A(256,256)
      S=0.0
      AN=FLOAT(NM)
      DO 20 J=ID1,ID2
        AM=AMEAN(J,NM)
        S1=0.0
        DO 10 I=1,NM
          S1=(A(I,J)-AM)**2+S1
 10     CONTINUE
        S1=S1/AN
        S=S+S1
 20   CONTINUE
      S=S/(ID2-ID1)
      SD=SQRT(S)
      RETURN
      END
C
C     ---------------------------------------------------------------------
C
C       THIS SUBROUTINE CALCULATES THE ROUGHNESS COEFFICIENT.
C
C     --------------------------------------------------------------------
C
      SUBROUTINE RC(R,NM)
      COMMON A(256,256)
      AIO=0.0
      AIT=0.0
      DO 20 J=1,256
C
C       Calculate the non-scattered intensities.
C
        AIO1=A(128,J)+A(129,J)+A(127,J)+A(130,J)
        AIO=AIO+AIO1
C
C       Calculate the scattered intensities.
C
        AIT1=0.0
        DO 10 I=130,256
          AIT1=A(I,J)+AIT1
10      CONTINUE
```

```
        AIT=AIT+2*AIT1
20    CONTINUE
C
C       Calaulate the roughness coefficient.
C
      R=AIT/AIO
      RETURN
      END
```

VITA

Cheng Luo was born in Shanghai, P.R.China, on March 30, 1959. He attended Qing Fong high school in Shanghai, P.R.China, and graduated in August 1976. In February 1978, he entered the China Textile University (CTU) in Shanghai, P.R.China. Upon graduating from CTU in 1982 with a Bachelor of Science degree in Textile Engineering, he was employed full time CTU as an instructor. During that time, Cheng was primarily engaged in the research of Air-jet spinning, carding and textile instrumentation. Besides, he was also responsible for the courses in Textile Engineering. Cheng left after working for CTU for approximately four years, and entered the Graduate School of the Kansas State University to pursue a Master of Science in Textile Science. In January 1987, he transferred to the University of Tennessee at Knoxville and received Master's degree with a major in Textile Science in May 1989.

Cheng is a member of the Society of China Textile Engineers, American Association of Textile Chemists and Colorist. His current plan is to continue his work at the University of Tennessee, in order to receive his doctorate.